Master Degree in Aerospace Engineering

April 2020

Master Thesis

Aerodynamic and Thermal Analysis of underhood of electric Hypercar

Academic Supervisor

Prof. Domenic D'Ambrosio

Candidate

Giacomo Gentile

Company Supervisors

Eng. Gabriele Velenich
Eng. Gianluca Francesconi

And so you touch this limit, something happens
and you suddenly can go a little bit further.
With your mind power, your determination,
your instinct, and the experience as well,
you can fly very high.
- ***Ayrton Senna***

Contents

Abstract **1**

1 Introduction **7**

1.1 AMET 7

1.2 Purpose of study 8

2 Theoretical Background **10**

2.1 Governing Equations of Fluid Dynamics 10

2.1.1 Continuity Equation 12

2.1.2 Momentum Equation 12

2.1.3 Energy Equation 13

2.1.4 Closure problem 14

2.2 RANS Equations 15

2.3 Near-wall treatment 17

2.3.1 Aerodynamic Boundary Layers 17

2.3.2 Thermal Boundary Layers 18

3 Electric Mobility **20**

3.1 Global EV Outlook 20

3.2 Rimac Automobili 20

3.2.1 Rimac C_Two 22
3.2.2 Front Underhood Compartment 23

4 Methodology **31**
4.1 Difference between FVM and FEM 32
4.2 AcuSolve Software 33
4.3 Set-up 34
4.3.1 Mesh 35
4.3.2 Spalart-Allmaras Turbulence Model 39
4.3.3 Physics Continua Model 40
4.3.4 Solver Setting 41

5 Base Model Preliminary Analysis **45**
5.1 First test case 49
5.2 Second test case 50
5.2.1 External Aerodynamics Model 50
5.2.2 Boundary conditions setting 53
5.3 Third test case 55
5.3.1 First Half of Car Model 55
5.3.2 Boundary conditions setting 56

6 Results **58**
6.1 Base Model 58
6.2 Optimized Models 62
6.2.1 Bottom Inlets 62
6.2.2 Front Inlet 69

7 Conclusions **79**

Acknowledgement **82**

Bibliography **84**

Abstract

Electric mobility is growing year by year becoming the alternative to traditional transport. In this window, also the major automotive companies of luxury cars, as Rimac Automobili, are moving to conquer this new market share. To ensure the best performance, the C_Two battery pack has to provide the right power to powertrain components that have to work within the operational temperatures without exceeding the survival limits. In addition to the internal liquid cooling systems, for some of the components we have to increase the heat transfer using the compartment air through force convection. To achieve this purpose, a new methodology has been implemented with AcuSolve software because of the availability of the solver by Rimac Automobili. The interesting peculiarity lies in the fact that the code is based on the Finite Element Method while most CFD codes are based on the Finite Volume discretisation. The pre-processing operations involve the use of BETA CAE ANSA and HyperMesh software which is part of the Altair Suite. The physical model is characterized by the RANS equations, that represent the right compromise between accuracy and computational cost, and the Spalart-Allmaras turbulence model which is robustly implemented in AcuSolve. Although the simulation results led to the compartment optimization, Altair Suite showed limits in the handling of the model and in the time used to elaborate any single operation; moreover, the computational time and CPU resources are higher than the competitors.

List of Tables

4.1 Surface mesh 37
4.2 Volume mesh 38
4.3 Boundary layers mesh 38
4.4 Steady State Problem description 42
4.5 Steady-State Solver setting 43
4.6 Transient Problem description 43
4.7 Transient Solver setting 43

5.1 Temperature table. 48
5.2 Boundary conditions of first test case. 49
5.3 External aerodynamics setting. 51
5.4 External aerodynamics boundary conditions. 51
5.5 Boundary conditions of second test case. 54
5.6 Boundary conditions of third test case. 57

6.1 Mass flow rates from the bottom inlets. 63
6.2 Mass flow rates from the front inlet 70

List of Figures

1.1 CFD scene by AMET. 7

1.2 Rimac C_Two. 8

2.1 Inner Boundary Layer. 18

2.2 Thermal Boundary Layer. 19

3.1 Example of sub-systems produced by Rimac 21

3.2 Rimac Automibili Concept One. 21

3.3 Rimac Automibili C_Two. 22

3.4 Front underhood of C_Two. 24

3.5 C_Two Motors. 24

3.6 C_Two Integrated Gearboxes. 25

3.7 C_Two Inverter. 25

3.8 C_Two PDM. 26

3.9 C_Two HVAC AC Compressor. 26

3.10 C_Two Cabin heat exchanger. 27

3.11 C_Two PTC heater. 27

3.12 C_Two Water pump. 28

3.13 C_Two Electrical power steering pump. 28

3.14 C_Two ABS and Brake front system units. 29

3.15 C_Two Steering system. 29

3.16 C_Two TPMS sensor. 30

4.1 Simplified front compartment model. 34

4.2 Underhood components after geometry clean up operations. 35

4.3 Meshing workflow. 36

4.4 Boundary layer generated by HyperMesh. 38

5.1 C_Two front underhood. 45

5.2 Front underhood components. 46

5.3 Inlets and outlet of the first test case. 49

5.4 Rimac C_Two CFD model. 50

5.5 Rimac C_Two CFD model details. 51

5.6 Cp field on Rimac C_Two 52

5.7 Pressure field on Inlets and Outlets 53

5.8 Inlets and outlet of the second test case. 54

5.9 Front section car of Rimac C_Two. 55

5.10 Front section car with the whole compartment 55

5.11 Pressure field on Inlets and Outlets 56

5.12 Inlets and outlet of the third compartment model. 57

6.1 Base model with plenum. 58

6.2 Global and Local Target Temperature on Gearboxes and motors XY section. 59

6.3 Global and Local Target Temperature on Gearboxes and Inverter XZ section. 60

6.4 Global and Local Target Temperature on Symmetry plane XZ section. 60

6.5 Global and Local Target Temperature on Gearboxes, PDM unit and motors YZ section 61
6.6 Global and Local Target Temperature on Gearboxes, PDM unit and motors YZ section 2. 61
6.7 Velocity on different sections. 62
6.8 Bottom inlets. 63
6.9 Bottom inlets velocities. 64
6.10 Global Target Temperature on Gearboxes and motors XY section. . . 64
6.11 Global Target Temperature on Gearboxes and Inverter XZ section. . 65
6.12 Global Target Temperature on Symmetry plane XZ section. 65
6.13 Global Target Temperature on Gearboxes, PDM unit and motors YZ section 1. 66
6.14 Global Target Temperature on Gearboxes, PDM unit and motors YZ section 2. 66
6.15 Local Target Temperature on Gearboxes and motors XY section. . . . 67
6.16 Local Target Temperature on Gearboxes and Inverter XZ section. . . 67
6.17 Local Target Temperature on Symmetry plane XZ section. 68
6.18 Local Target Temperature on Gearboxes, PDM unit and motors YZ section 1. 68
6.19 Local Target Temperature on Gearboxes, PDM unit and motors YZ section 2. 69
6.20 Front inlet. 70
6.21 Global Target Temperature on Gearboxes and motors XY section. . . 71
6.22 Global Target Temperature on Gearboxes and Inverter XZ section. . 71
6.23 Global Target Temperature on Symmetry plane XZ section. 72

6.24 Global Target Temperature on Gearboxes, PDM unit and motors YZ section 1. 72
6.25 Global Target Temperature on Gearboxes, PDM unit and motors YZ section 2. 73
6.26 Local Target Temperature on Gearboxes and motors XY section. . . . 73
6.27 Local Target Temperature on Gearboxes and Inverter XZ section. . . 74
6.28 Local Target Temperature on Symmetry plane XZ section. 74
6.29 Local Target Temperature on Gearboxes, PDM unit and motors YZ section 1. 75
6.30 Local Target Temperature on Gearboxes, PDM unit and motors YZ section 2. 75
6.31 TPMS respect the Global Target Temperature. 76
6.32 Outlets Mass Flow rates. 77
6.33 Inlets Mass Flow rates. 77
6.34 Side inlets velocity. 78
6.35 Top inlets velocity. 78

Chapter 1

Introduction

1.1 AMET

AMET is a high-tech engineering company established in 1999 with its headquarters in Turin (Italy). It has grown over the years opening other two subsidiaries in Italy, Modena and Naples, one in the USA, Detroit, and one in the Slovak Republic, Kosice.

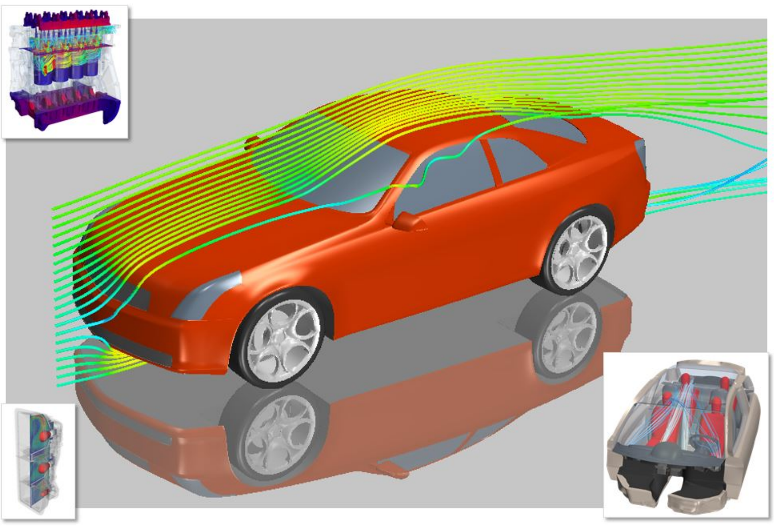

Figure 1.1: CFD scene by AMET.

AMET operates in several fields, mainly in the transport sector(automotive, aerospace and railways) but also in robotics, marine and white goods sectors. In fact, it is able to offer a wide range of virtual analysis, such as CAE structural simulations and optimizations (CFD, Crash, MB, NVH) [Fig. 1.1], automatic controls design, consulting (e.g. weight management and data analysis) and also tools for experimental tests (e.g. fatigue, hardware-in-the-loop); moreover it collaborates with Universities, Research Institutes and costumers to develop research and innovation activities [1].

1.2 Purpose of study

The thesis aims to find a new methodology with a FEM code, in particular with ***Altair*** CFD software, *AcuSolve*. This choice has been led by the fact that it is included in the suite with no added cost and also because it can solve Direct Coupled Fluid-Structure Interactions [2].

In order to explore the potentiality of the software, it has been decided to analyse the aero-thermal field in the front powertrain compartment of the ***Rimac Automobili C_ Two***, showed in figure 1.2.

Figure 1.2: Rimac C_Two.

Due to the presence of several electric and mechanical components, it is necessary to prevent their overheating through the optimization of the airflow inside the compartment to ensure that the local temperature is lower than a predefined threshold in the worst scenario.

To achieve the purpose, the commercial software ***Beta CAE*** *ANSA* Pre-processor has been used for the geometry clean up operations due to its capacity to deal with complex geometries. The meshing process - creation of surface and volume mesh - was implemented directly on the commercial pre-processor ***Altair*** *HyperMesh* in order to have a direct link with AcuSolve.

Chapter 2

Theoretical Background

The importance of Fluid Dynamics lies in the fact that every physical entity is involved with some type of fluid. In primis, one could think that it is relevant exclusively in the automotive, aerospace and aeronautical fields but, actually, many different sectors are beginning to approach to these concepts. An example is the Civil Engineering which uses Fluid Dynamics to study the stiffness and flexibility of skyscrapers under wind load.

Any fluid flow is governed by three conservation laws: mass, momentum and energy. These laws can be expressed in mathematical form using the Navier-Stokes equations. Due to their high non-linearity, they do not have analytical solutions, excepts for simple cases. The role of Computational Fluid Dynamics (CFD) is to find a numerical way to discretize and solve Navier-Stokes equations [3].

2.1 Governing Equations of Fluid Dynamics

The Navier-Stokes Equations describe a thermodynamically open system which takes in account the losses due to viscosity. They express the following laws:

- Conservation of Mass;
- Conservation of Momentum;

- Conservation of Energy.

This approach is possible only if we consider valid the following hypothesises:

- Continuous flow;
- Non-reacting and homogeneous flow;
- Flow without electric particles.

The first one deals with the concept of Mean Free Path that is the average distance travelled by a particle between two successive impacts; the Kinetic Theory of Gas gives the following result for a mono-component gas made by spherical and not attractive molecules in equilibrium conditions:

$$\lambda = \frac{1}{\sqrt{2}\pi d^2 n} \tag{2.1.1}$$

where,

- d, collision diameter;
- n, number density (particles per unit volume).

This physic parameter is important to understand the type of flow we are analysing; in fact, the continuum concept is linked to the comparison between the subsequent impacts and the motion of the center of gravity of a set of molecules in traveling along a characteristic length L of a body immersed in the fluid. All this concepts are summarised by the Knudsen number:

$$K_n = \frac{\lambda}{L} \tag{2.1.2}$$

Depending on the value of it, we can have several flow conditions:

- $K_n < 0.01$, Continuous Flow;
- $0.01 < K_n < 0.1$, Slip Flow (Slightly rarefied);
- $0.1 < K_n < 10$, Transition Flow (Moderately rarefied);
- $K_n > 10$, Free molecular Flow (Highly rarefied);

Based on these concepts, it is assumed that the flow is continuous and composed by the sum of Fluid Particles. A single one is a set of molecules that need to be enough big to present same statistic thermodynamic values and enough small to be almost point-like; therefore, in this way, we can describe the evolution of the flow in terms of velocity, pressure, temperature, density, enthalpy and viscosity in each point.

2.1.1 Continuity Equation

The first law is the continuity equation that originates from Lavoisier's postulate: *"Nothing is created, nothing is destroyed, everything is transformed."*. In fact, it expresses the net flux of mass coming out from the arbitrary control volume through its surface. What has been said is clarified by the following scalar partial differential equation:

$$\frac{\partial \rho}{\partial t} + \overline{\nabla} \cdot \left(\rho \overline{V}\right) = 0 \tag{2.1.3}$$

where,

- ρ, Density of the fluid;
- $\overline{V}$, Velocity vector (u**i**+v**j**+w**k**).

2.1.2 Momentum Equation

The second equation derives from Newton's second law of motion and it states that the net change of momentum in any direction is due to the sum of the pressure, dissipative and body forces exerted. What has been said is clarified by the following vectorial partial differential equation with the same assumptions as before:

$$\frac{\partial\left(\rho\overline{V}\right)}{\partial t}+\overline{\nabla}\cdot\left(\rho\overline{V}\overline{V}\right)=-\overline{\nabla p}+\overline{\nabla}\overline{\overline{\tau}}+\rho\overline{f} \tag{2.1.4}$$

where,

- ρ, Density of the fluid;
- $\overline{V}$, Velocity vector (u**i**+v**j**+w**k**);
- $\overline{\overline{\tau}}$, Stress Tensor;
- p, Pressure.
- $\overline{f}$, Body Forces.

2.1.3 Energy Equation

The third equation takes into account the rate of change of the total energy owing to the net heat flux towards the control volume plus work done per time unit on the control volume by volumetric and surface forces. What has been said is clarified by the following scalar partial differential equation:

$$\frac{\partial E}{\partial t}+\overline{\nabla}\cdot\left(E\overline{V}\right)=\rho\dot{\xi}-\overline{\nabla}\cdot\dot{\overline{q}}-\overline{\nabla}\cdot\left(p\overline{V}\right)+\overline{\nabla}\cdot\left(\overline{\tau}\cdot\overline{V}\right)+\rho\overline{f}\cdot\overline{V} \tag{2.1.5}$$

here,

- $\dot{\xi}$, Heat Absorbed per unit time and unit mass;
- $\dot{\overline{q}}$, Heat Flux due to thermal conduction where k is the conduction constant;
- $E=e+\frac{\left|\overline{V}\right|^2}{2}$, Total Energy per unit volume as sum of internal energy e and kinetic energy;
- $p\overline{V},\overline{\tau}\cdot\overline{V},\rho\overline{f}\cdot\overline{V}$, Work done by Pressure, Viscosity Dissipation and Body Forces.

2.1.4 Closure problem

As it is possible to note, the Navier-Stokes laws are 5 equations in 14 unknowns:

- ρ, Density;
- u_i, three components of Velocity;
- p, Pressure;
- T, Temperature;
- τ_{ij}, six components of Stress Tensor;
- e, Internal Energy;
- μ, Viscosity.

For this reason it is necessary to add other equations to close the problem. The temperature can be expressed through the Ideal Gas law:

$$T = \frac{p}{\rho R^*} \tag{2.1.6}$$

with $R^* = \dfrac{R}{M}$ where R is the universal gas constant and M is the molar mass. The Stress Tensor, indeed, derives by the viscosity Newton's law:

$$\tau_{ij} = \mu \left(\frac{\partial u_i}{\partial x_j} + \frac{\partial u_j}{\partial x_i} \right) \tag{2.1.7}$$

where μ is the dynamic viscosity of the fluid which, in turn, depends on pressure and temperature: $\mu = \mu\,(p, T)$. At the end, the Internal Energy is a function of Temperature and it is stated as: $e = c_v T$, where c_v is the Specific Heat considering constant volume. Now, the problem is a closed system but, unfortunately, there is not any analytical solution; only in some rare and really simple cases.

2.2 RANS Equations

In real phenomena, most flows are turbulent and they can be characterized by several properties:

- Highly unsteady condition;
- Three dimensional;
- Vortex stretching, which increases turbulence;
- Mixing, which leads to turbulent diffusion and to a dissipative process that converts kinetic energy into internal energy;
- Coherent structures, which are responsible for a large part of mixing;
- Wide range of length and time scales.

In cases where high heat transfer is needed, it is useful to have mixing phenomenon; so to cool hot components is preferable to have turbulent flows around them.

The Navier-Stokes equations are able to describe any type of turbulent flows. Consequently, it should be possible to use the DNS (Direct Numerical Simulation) approach but the computational time increases considerably with respect to the following approach despite it is more exact.

A normal engineering approach is to use the Reynolds-Averaged-Navier-Stokes equations which are applied when the flow is statistically steady. In this condition every variables can be written as the sum of a time-averaged value and a fluctuation:

$$\phi(x_i, t) = \overline{\phi(x_i)} + \phi'(x_i, t) \tag{2.2.1}$$

where

$$\overline{\phi(x_i)} = \lim_{T\to\infty} \frac{1}{T} \int_0^T \phi(x_i, t)\, dt \tag{2.2.2}$$

with t equals to time and T to averaging interval, which has to be larger than the typical time scale of the fluctuations. In this way, the variable does not depend on the time at which the averaging is begun.

Applying the Reynolds decomposition to the Navier-Stokes equations, the averaging fluctuations are null while from the quadratic quantities two new terms are obtained:

$$\overline{u_i\phi} = \overline{\left(\overline{u}_i + u_i'\right)\left(\overline{\phi} + \phi'\right)} = \overline{u}_i\overline{\phi} + \overline{u_i'\phi'} \tag{2.2.3}$$

Introducing the 2.2.3 in the conservations equations for an incompressible flow, we obtain:

$$\overline{\nabla} \cdot \overline{V} = 0 \tag{2.2.4}$$

$$\frac{\partial \overline{u_i}}{\partial t} + \frac{\partial}{\partial x_j}\left(\overline{u_i u_j}\right) + \frac{\partial}{\partial x_j}\left(\overline{u_i' u_j'}\right) = -\frac{\partial \overline{p}}{\partial x_i} + \mu \frac{\partial}{\partial x_j}\left(\frac{\partial \overline{u}_i}{\partial x_j} + \frac{\partial \overline{u}_i}{\partial x_j}\right) - \frac{\partial}{\partial x_j}\left(\rho\overline{u_i' u_j'}\right) \tag{2.2.5}$$

The term $-\rho\overline{u_i' u_j'}$ is the ***Reynolds stress tensor*** which is symmetric and consequently there are six independent terms and it represents the momentum transfer due to the velocity fluctuations. It means that the problem is not closed and, consequently, some approximations are needed to prescribe them in terms of the mean quantities. They are the ***Turbulence models*** [4] and, in particular, in this work has been used the one-equation model, **Spalart-Allmaras**, which has been deepened in the cap. 4.

2.3 Near-wall treatment

Since fluids, as air, have low viscosity, they are high Reynolds flows and, therefore, they have an ***asymptotic behaviour*** of dimensionless coefficients. Consequently, these flows can be divided into two macro-regions: inviscid outer flow and **boundary layer**, that is the thinner area close to the walls where the viscosity is predominant generating vorticity. The latter can be *Aerodynamic* or *Thermal*.

2.3.1 Aerodynamic Boundary Layers

Having an asymptotic behaviour, the boundary layer can be studied through dimensionless variables; in fact this property is called **Wall Similarity**. These are necessary to describe uniquely the characteristic scales of viscosity fluctuations in the aforementioned region [5]. To find them, friction viscosity u_τ and scale length l_ν are introduced:

$$u_\tau = \sqrt{\frac{\tau_w}{\rho}} \qquad l_\nu = \frac{\nu}{u_\tau} \tag{2.3.1}$$

where τ_w is the *wall stress* computed by Newton's law and, through these variable, is possible to evaluate the non-dimensional velocity and length, called *inner variables*:

$$u^+ = \frac{u}{u_\tau} \qquad y^+ = \frac{y}{l_w} = \frac{u_\tau y}{\nu} \tag{2.3.2}$$

While the laminar boundary layer is relatively simple to compute because it is a mono layer, the turbulent layer is more complicated. The boundary layer is divided into an *outer layer*, which connects it to the undisturbed flow, and *inner layer*, which is a multi-layer [2.1] as follows:

1. **Pure Viscous Sublayer**: $0 \leq y^+ \leq 5$ $\quad u^+ = y^+$

   in this region the viscous forces are predominant over the inertial ones (low Re);

2. **Buffer Layer**: $5 < y^+ < 30$

   it is a mixing zone where there is the maximum production of turbulent kinetic energy and the viscous and inertial forces are comparable;

3. **Logarithmic Layer**: $y^+ > 30$ $u^+ = \frac{1}{k} ln\,(y^+) + C^+$

   where $k = 0.41$ is the *Von Karman constant* and $C^+ = 5$ is the *Coles constant*; the inertial forces become predominant over the viscous ones (high Re).

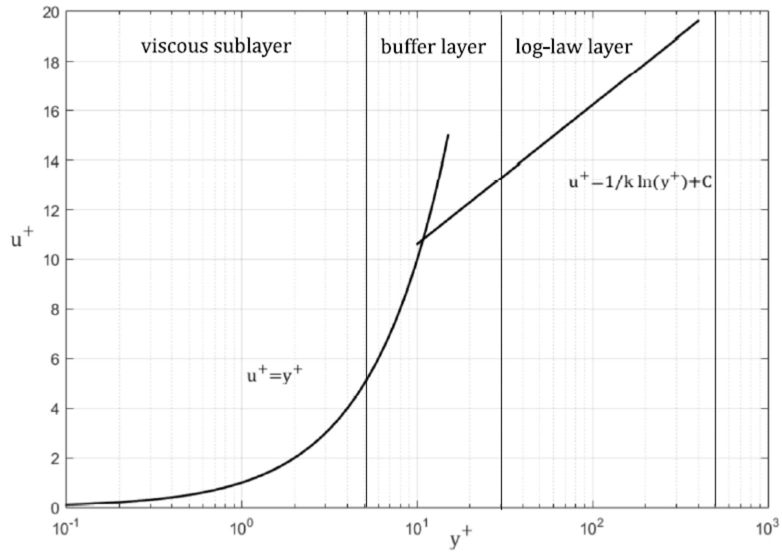

Figure 2.1: Inner Boundary Layer.

2.3.2 Thermal Boundary Layers

Due to the fact that air physical properties depend on temperature and pressure, it is necessary to couple the velocity field to temperature one. Consequently, the buoyancy forces in the gravity field appear in the conservation equation. This represents the **Natural Convection** while, when properties do not depend on the aforementioned variables, there occurs the **Forced Convection**. Indeed, when both are, we speak of **Mixed Convection**.

In many natural convection cases, it is possible to consider only the temperature dependence of the properties, e.g. constant pressure flows. If the heat fluxes at the wall are moderate, the physical characteristics can be described by linear functions of temperature.

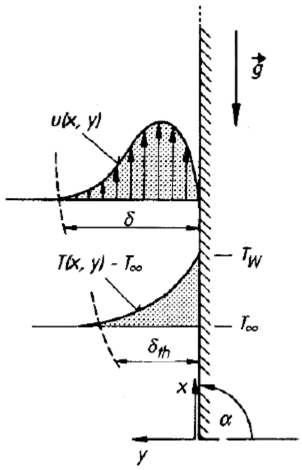

Figure 2.2: Thermal Boundary Layer.

The heat transferred from the walls to the fluid implicates a local increasing of temperature and, in turn, a change of density; this is the origin of natural convection. The effect is restricted to a thin region near the wall and its thickness δ_{th} is equal to the distance along the normal of the wall at which the temperature is over the undisturbed one: $T > T_\infty$ [6].

Chapter 3

Electric Mobility

3.1 Global EV Outlook

For the year 2020, the European Union (EU) has fixed the objectives to reduce energy consumption by 20%, to reduce the greenhouse emissions by 20% and to obtain 20% of total energy consumption by renewable energy sources. In order to decrease the use of fossil fuels in urban mobility and improve air quality and energy efficiency the presence of Electric Vehicles (EV) on the streets is promoted by EU green polices [7].

Generally electric road cars have the disadvantage of insufficient autonomy due to the capability of the battery pack. This is one of the most important reasons why there are a few electric super cars. This challenge has been accepted by Rimac Automobili in order to create an hyper car capable to ensure a good autonomy (about 550 km) but high performance comparable to the same ICE (Internal Combustion Engine) category.

3.2 Rimac Automobili

Rimac Automobili was founded in Croatia in 2009 with the idea to design and produce the sportcars of the future. Soon, it was clear that it first had to design and develop the various sub-systems [Fig. 3.1] unleashing the full potential of Nikola Tesla's inventions.

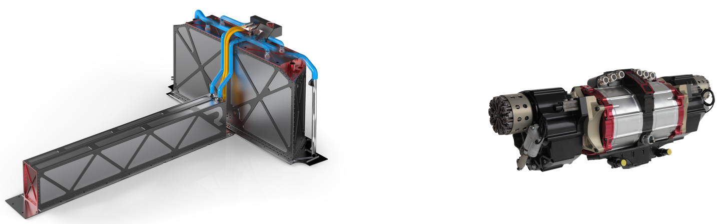

(a) *Concept One Battery Pack* (b) *Concept One Powertrain*

Figure 3.1: Example of sub-systems produced by Rimac

In 2011, it exhibited the first full electric supercar, the Concept One, at the Frankfurt Motor Show [Fig. 3.2]. In few years it has attracted several investments that led, in 2014, to be the FIA Formula E official Race Director Car and to produce the Concept S and the E-Runner Concept One.

Figure 3.2: Rimac Automibili Concept One.

With this global exposure, the brand has grown up calling in famous investors as Porsche Engineering Group in order to develop together the electric cars of Volkswagen Group, Camel Group to study mainly batteries and Hyundai Motor Group to design new high performance electric cars.

3.2.1 Rimac C_Two

Thanks to the aforementioned projects, a new star is being born: ***C_ Two***, [Fig. 3.3]. The Croatian Hypercar wants to be a new competitor for the most known brands creating a special car with incredible performance:

- Acceleration 0-60 mph in 1.85 sec;
- Max Speed equal to 412 kph;
- 1914 horsepower (1400 kW) distributed on 4 electric motors, one for each wheel;
- Active Aerodynamics.

Figure 3.3: Rimac Automibili C_Two.

3.2.2 Front Underhood Compartment

For Internal Combustion Engine cars, temperatures problems and cooling requests are known and many researches are carried on over the years. The Rimac C_Two is one of the first electric hyper-car in the world and a new approach to powertrain temperature management is needed.

Even though temperatures inside the underhood [3.4] are surely lower than those of the same ICE vehicle category, they could represent a serious problem for all the electrical and, above all, electronic components. These have stringent constraints in terms of temperature allowed to ensure the correct operation mode. An other problem is determined by the electromagnetic compatibility of a device; this property means that no Electromagnetic Interference (EMI) should be caused by the electromagnetic environment on the device and that the device does not create faults in others nearby [8]. In over temperature conditions, EMI problems appear and they can be really dangerous from a technical point of view damaging the components, but also it can cause unacceptable risks to passenger safety [9]. Moreover, among the most sensible components in the electric motor there are the insulations which are in contact with stator windings [10]. It is made by polymeric materials which deteriorate with the heat. Other critical component, probably more than motor itself, is the inverter which may suffer high temperature enough to fail. The necessity arises to investigate the thermal-dynamics behaviour of the powertrain compartment of the C_Two model in order to guarantee the maximum design performance, in every conditions of use, always looking for human safety.

The work has been focused, in particular, on the **Front powertrain compartment** because it is not completely equipped with a liquid-cooling system. It is clear that it is necessary a detailed study of the velocity and temperature fields inside the box that depend mostly on the external aerodynamics. Indeed, it allows to identify which are the inlets and outlets of the compartment analysing the pressure.

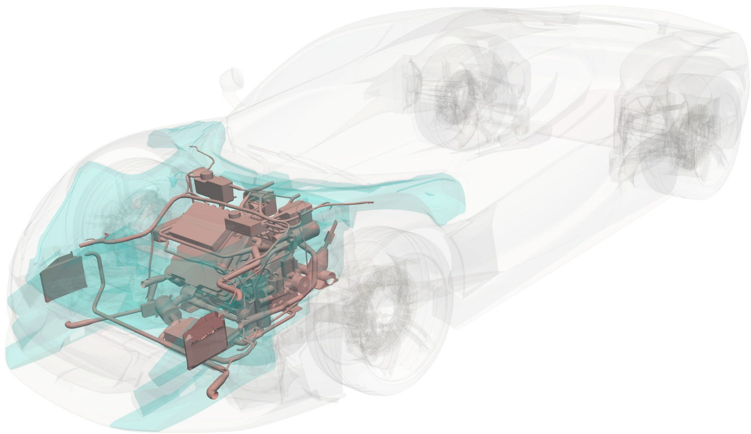

Figure 3.4: Front underhood of C_Two.

The compartment has been analysed in the worst scenario comparable to track condition where the main thermal stressed components, which are geometrically simplified, are as follows:

- **Motors**, one for each wheel and thanks to the oil-cooling they offer instant response ensuring excellent performance;

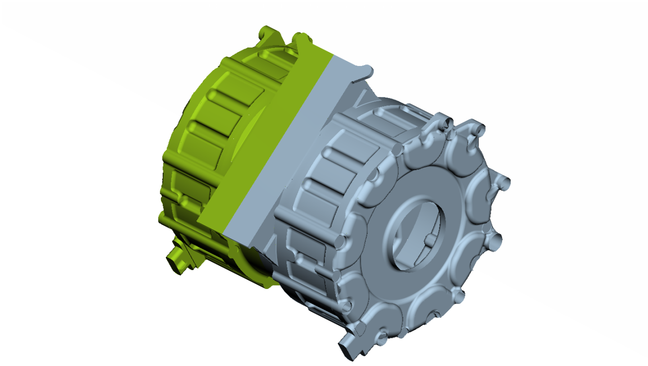

Figure 3.5: C_Two Motors.

- **Gearboxes**, one for each motor and they include a single speed system with dual carbon clutch and pulse dampening units;

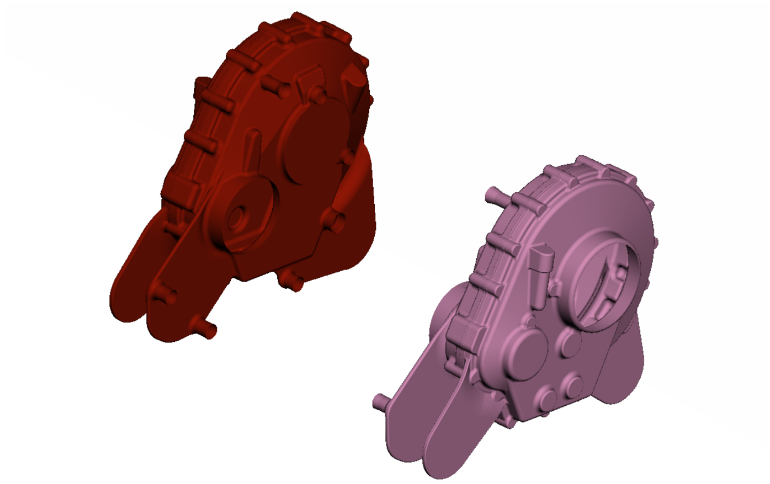

Figure 3.6: C_Two Integrated Gearboxes.

- **Inverter**, compact with the lowest weight but high peak current (up to 1000 ARMS) ensuring quality and durability;

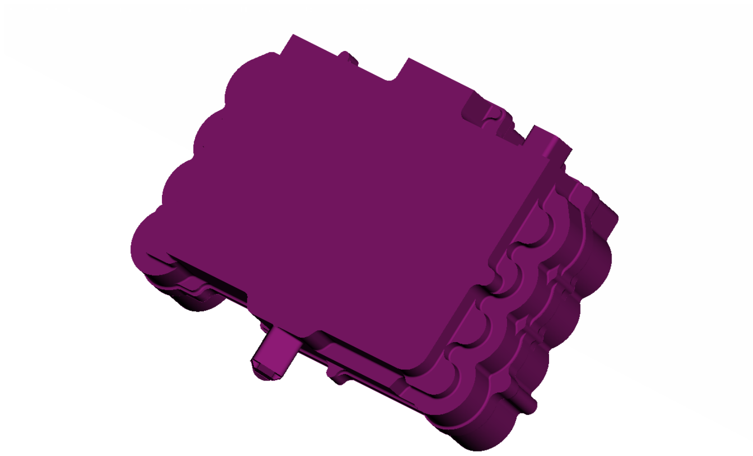

Figure 3.7: C_Two Inverter.

- **Power Distribution Module (PDM)**, used to provide electrical power from battery pack to motors.

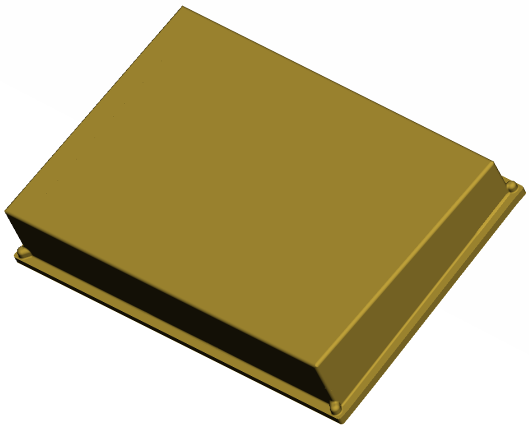

Figure 3.8: C_Two PDM.

- **HVAC AC Compressor**, needed to let the refrigerant flows to the lower pressure zone in the evaporator to ensure cabin temperature comfort.

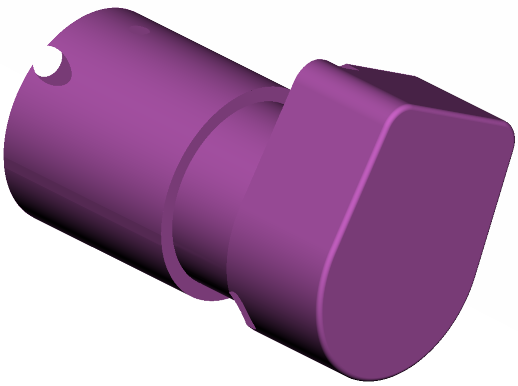

Figure 3.9: C_Two HVAC AC Compressor.

- **Cabin Heat Exchanger**, part of HVAC system, it allows heat exchange between electrical components (motors, inverters) and cabin.

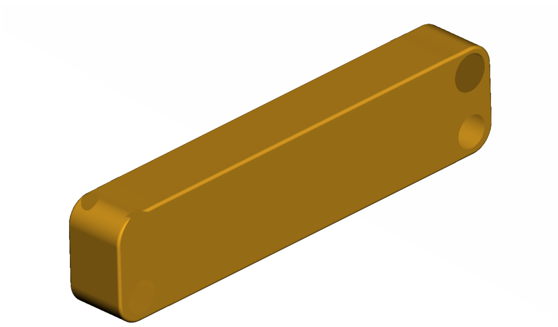

Figure 3.10: C_Two Cabin heat exchanger.

- **Positive Temperature Coefficient (PTC) Heater**, a self-regulating heater covered by conductive inks printed on thin, flexible polymer-based substrates. This material allows current to pass when it is cold while restricts it to flow as the temperature increases.

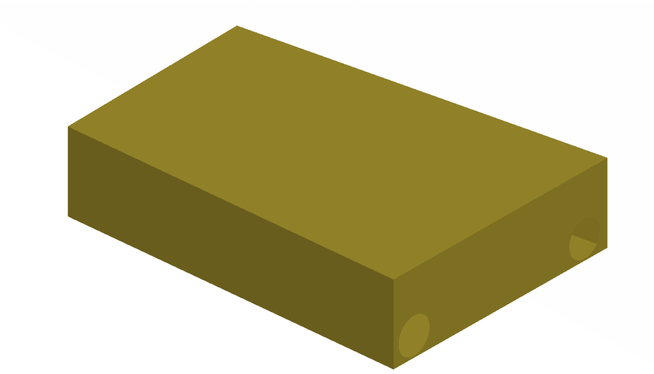

Figure 3.11: C_Two PTC heater.

- **Water Pump**, needed to circulate water in the tubes to cool the several systems.

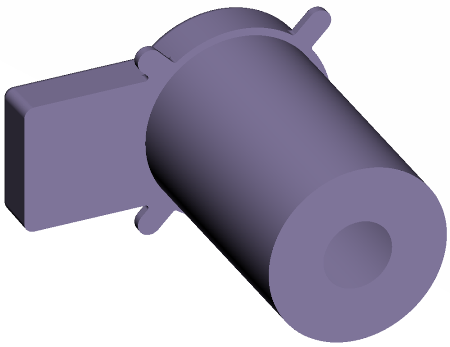

Figure 3.12: C_Two Water pump.

- **Electrical Power Steering Pump**, needed to circulate oil in the tubes of power steering system which helps the drivers to steer the vehicle augmenting steering effort.

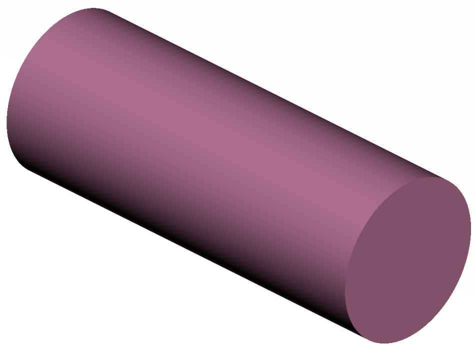

Figure 3.13: C_Two Electrical power steering pump.

- **ABS and Brake System Front Units**, a parts of brake system to control front wheels.

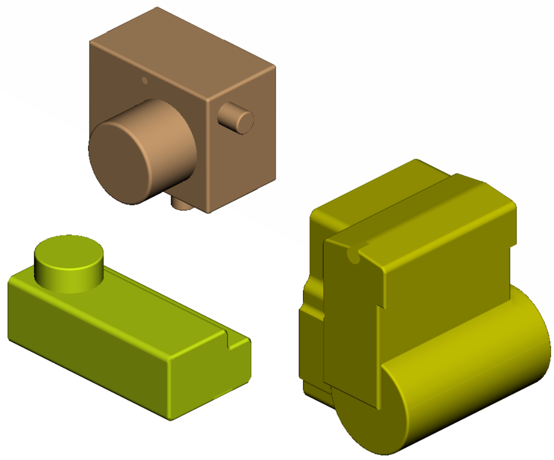

Figure 3.14: C_Two ABS and Brake front system units.

- **Steering System**, the part which allows steering the wheels and thus the car.

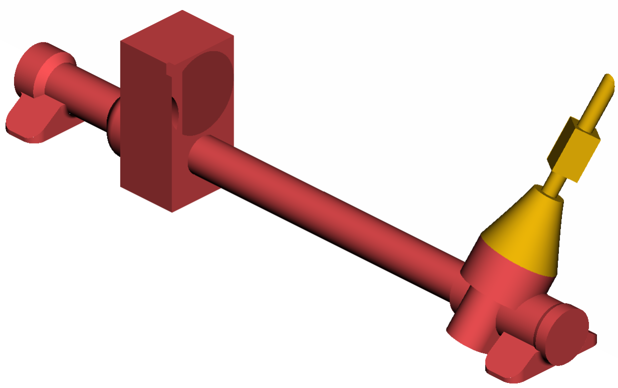

Figure 3.15: C_Two Steering system.

- **Tire-Pressure Monitoring System (TPMS) Sensor**, an electric system which allows to monitor tires air pressure.

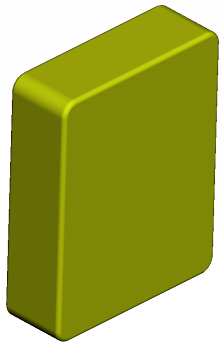

Figure 3.16: C_Two TPMS sensor.

Moreover, all the relative tubes and electrical cables have been taken into consideration [11].

Chapter 4

Methodology

Since an analytical approach is not possible, a numerical one is needed. Due to the ability of computer to work only with discrete information, the physical quantities, as space and time, but, also, the algebraic equations have to be discretized [12].

Basically, a numerical method is determined by the following components:

- *Mathematical model*, the set of partial differential equations (PDE) describing the physics;
- *Discretization method*, the way to discretize the previous chosen equations (i.e. mainly Finite Volume Method and Finite Elements Method in CFD uses);
- *Coordinate system*;
- *Numerical grid*, that is called Mesh;
- *Solution method*, the way to solve the PDE system.

The choice determines the goodness of the method in terms of:

- *Consistency*, the method should return a more exact solution, more is the mesh refinement;

- *Stability*, errors due to discretization should not amplify during the iterations;
- *Convergence*, the solution should tend to the exact equations solution;
- *Conservation*, the conservation laws should be verified in the discretized form;
- *Realizability*, all the phenomena, from simple to complex, should be modelled to ensure realistic solution.
- *Boundedness*, the numerical solution could oscillate but within the bounds.

All these properties should be modelled in order to guarantee the higher level of accuracy [4].

4.1 Difference between FVM and FEM

The **Finite Volume Method** starts from the integral form of the conservation equations, which are applied to each Control Volume used to discretize the solution domain. The conservation laws have to be fulfilled locally and globally. The values of each physical quantity are computed at the centroid of the control volumes and interpolation is used to express variables at the faces, representing the surface integrals. As a result, the Navier-Stokes equations are discretized in an algebraic system, considering centroid and neighbour nodal values in each equation. FVM is conservative by construction because close control volumes share the boundaries in which the surface integrals are the same. FVM is suitable for complex geometries because it can be adapted to any kind of computational grid and all the terms of the equations have a physical meaning. These are two main reasons why this method is very popular in engineering fields.

The **Finite Element Method** is similar to the previous one in the way in which the domain is divided in control volumes, with the difference that the equations are multiplied by a weight function before the integration. One of the advantages is the ability to deal with arbitrary geometries, using unstructured grids. The principal drawback relies in the difficulty to find efficient solution method due to the structure of the matrices of the linearised equations [4].

4.2 AcuSolve Software

The particularity of **AcuSolve** lies in being one of the few Finite Element codes. The method provides to find approximated values in the nodes through shape function for the variables over the domain. They are substituted into the conservation laws in the differential form and the residual error is minimized using a weighted residual approach. Consequently, this formulation transforms the governing equations into integral form, called global weak form.

A method to evaluate the weighted residuals is based on **Galerkin Least Squares (GLS) formulation**. Its success in structural applications is due to a particular weighted residual formulation. It leads to symmetric stiffness matrices and, in turn, to the minimum possible difference between the exact solution and the approximated one. This property is lost in the case of convective heat transfer because the matrix associated with convection term is non-symmetric. This is due to spurious node-to-node oscillations that appear when the downstream boundary condition forces a rapid change in the solution. To avoid this problem is needed to refine the mesh. This approach provides second order accuracy for spatial discretization of all variables and uses controlled numerical diffusion operators in order to achieve stability and maintain accuracy [13].

Regarding the solving of steady state simulation, the inertia terms of conservation equations are only included in Galerkin part and not in all ones of the weighted residual approach in order to raise the stability of non linear iterations. This exclusion is not respected in transient simulation because, including the inertia terms in all parts of the formulation, preserves the time accuracy.

The resultant equations system is solved as a fully coupled velocity-pressure matrix system ensuring robustness and rapid convergence on large unstructured meshes [2].

4.3 Set-up

In order to familiarize with the software, a fake simplified model of the front compartment [Fig. 4.1] has been used to test its capability and robustness. It is not representative of the real underhood, but it is just a geometrical sample considering only the main components in terms of temperatures and obstacles to the air. The aim is to have a reference model easy to manage in order to determinate the set-up to use for the thesis object.

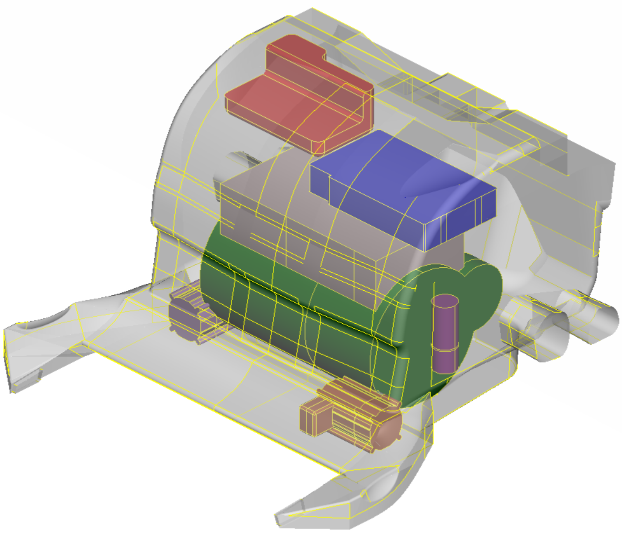

Figure 4.1: Simplified front compartment model.

The first step was to understand how to prepare the geometry in order to execute the mesh operation. Differently to other software, AcuSolve prefers to work with surfaces and it is not able to deal with compenetrations otherwise it can not run the volume mesh. Consequently, it has been necessary to apply geometry clean-up operations in order to ensure the right model for the surface meshing, as showed in figure 4.2:

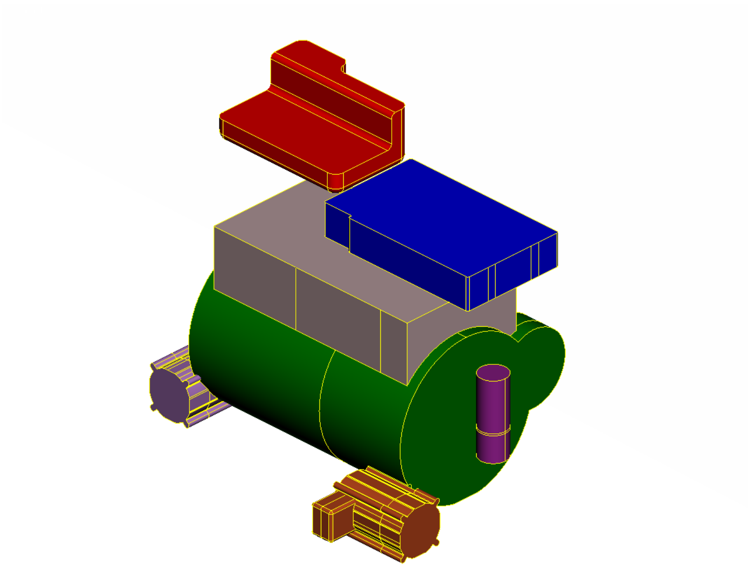

Figure 4.2: Underhood components after geometry clean up operations.

4.3.1 Mesh

After the geometry cleaning-up, the next step of process can be described through the loop showed in figure 4.3. The staring point is the *Surface Mesh* which has to be properly refined in the most critical zones, for example between neighbouring components or interesting zones, while it can be rough where there are not significant gradients in the physical quantities of interest.

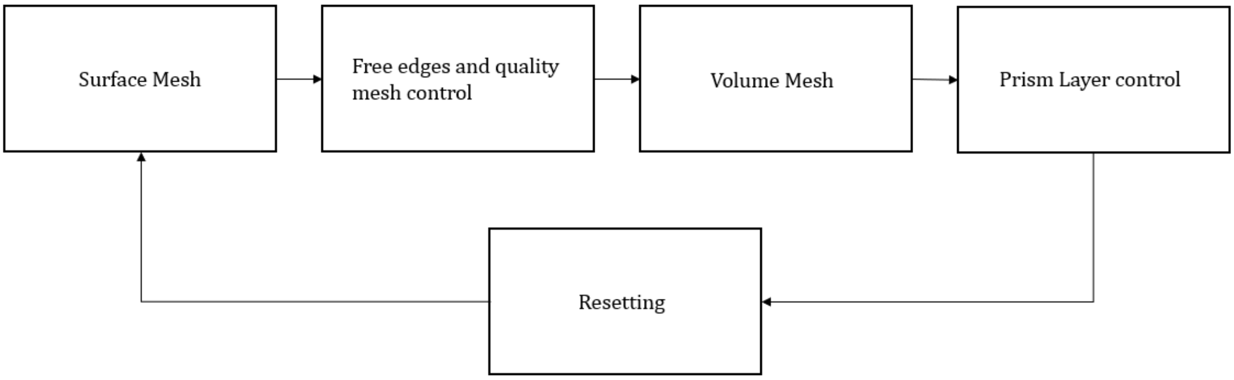

Figure 4.3: Meshing workflow.

Its quality is really important because, differently to other codes, the prepared mesh is not remeshed automatically by HyperMesh according to some own optimizing functions. In order to achieve this goal, the **Surface Deviation** algorithm has been used, where it is possible to decide the following parameters:

- Minimum size;
- Maximum size;
- Growth rate;
- Maximum deviation, allows to control the distance between the created elements and the surface and decreasing it means to reproduce better the geometry;
- Maximum feature angle, allows to set the maximum angle between two following elements and decreasing it means to increase accuracy of the mesh.

During this mesh sensitivity operations, it drew notice that over a determined number of million of nodes the solution does not change while it increases only the computational cost. Consequently, the surface mesh model is chosen as follows [4.1]:

Table 4.1: Surface mesh

Properties	Value
Min size	1 mm
Max size	60 mm
Growth rate	1.1
Max deviation	0.05
Max feature angle	10°

Later, it is the moment of the *Volume Mesh.* Through the Mesh Controls panel is possible to set the correct path to follow in order to obtain only the fluid volume selecting the options:

1. **Volume selector**,which allows to choose the elements belonging to fluid;
2. **Tetra + BL**, as Model which allows to generate a tetra-mesh with the Boundary Layers;
3. **No BL**, as Local control which allows to disable the prism layers around some components, for example the inlet/outlet surfaces.

Assuming a certain velocity inside the compartment a first possible thickness of boundary layer around the components has been determined but after the simulation, it has been changed according to the relative velocity results. Applying this concept iteratively, it has been possible to size it properly, also taking into account where two or more devices were too close, in order to achieve a good convergence and physical results.

The consequence of this process is described in the following table 4.2:

Table 4.2: Volume mesh

Properties	**Value**
Min size	1 mm
Max size	60 mm
Growth rate	1.4

while the characteristics of the boundary layers are in the table 4.3:

Table 4.3: Boundary layers mesh

Properties	**Value**
Number of layers	5
First layer height	0.13 mm
Total thickness	1 mm

These values are the general parameters applied into the general model but, obviously, in the areas where several components were too close, it has been necessary to use another algorithm for the prism layers. It generates the first layer as a percentage of the selected surface mesh size and, in this way, it has been possible not to collapse prisms by refining the elements in the interesting zones.

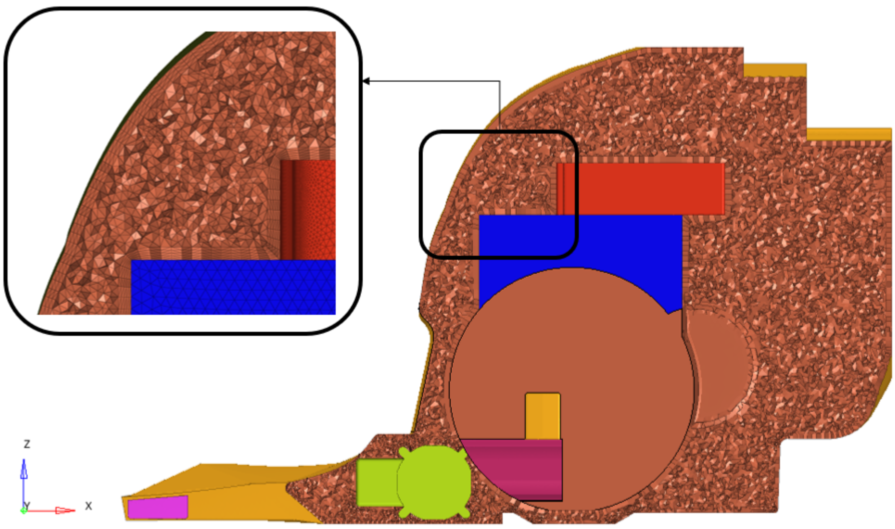

Figure 4.4: Boundary layer generated by HyperMesh.

4.3.2 Spalart-Allmaras Turbulence Model

As aforementioned the RANS equations need some turbulence model to close the problem. The Reynolds stress tensor has, in the principal axes, null the shear stresses while equal to eigenvalues the normal stress, thus it is symmetric positive semi-definite. The distinction between shear and normal stress depends on the chosen coordinate system but it is possible to make another distinction between isotropic and anisotropic stresses. Indeed, the isotropic stress is $\frac{2}{3}k\delta_{ij}$, where $k = \frac{1}{2}\overline{u_i'u_i'}$ is the *Turbulent Kinetic Energy* and the deviatoric anisotropic one is:

$$a_{ij} = \overline{u_i'u_j'} - \frac{2}{3}k\delta_{ij} \tag{4.3.1}$$

Consequently, the normalized anisotropy tensor is defined by:

$$b_{ij} = \frac{a_{ij}}{2k} = \frac{\overline{u_i'u_j'}}{\overline{u_i'u_i'}} - \frac{1}{3}\delta_{ij} \tag{4.3.2}$$

From these definitions, the **Reynolds Stress Tensor** derives as follow:

$$\overline{u_i'u_j'} = \frac{2}{3}k\delta_{ij} + a_{ij} \tag{4.3.3}$$

but only the anisotropic component a_{ij} is responsible for the momentum due to the fluctuations while the isotropic one is absorbed in a modified mean pressure.

In 1877 Bousinessq introduced the **turbulent-viscosity hypothesis** which provides for the deviatoric anisotripc component is proportional to:

$$-\rho\overline{u_i'u_j'} + \frac{2}{3}\rho k\delta_{ij} = \rho\nu_T\left(\frac{\partial\overline{u_i}}{\partial x_j} + \frac{\partial\overline{u_j}}{\partial x_i}\right) = 2\rho\nu_T\overline{S_{ij}} \tag{4.3.4}$$

where the ν_T is called **Turbulent (or Eddy) Viscosity**. Substituting into the mean-momentum equation, it is obtained as follows:

$$\frac{\partial \overline{u_i}}{\partial t} + \frac{\partial}{j}\left(\overline{u_i u_j}\right) = -\frac{1}{\rho}\frac{\partial}{i}\left(\overline{p} + \frac{2}{3}\rho k\right) + \frac{\partial}{\partial x_j}\left[(\nu + \nu_T)\left(\frac{\partial \overline{u_i}}{\partial x_j} + \frac{\partial \overline{u_j}}{\partial x_i}\right)\right] \tag{4.3.5}$$

where $\nu_{eff} = \nu + \nu_T$ is the **Effective Viscosity** and the pressure term is slightly modified due to the presence of $\frac{2}{3}\rho k$ [14].

In 1994 Spallart and Allmaras described a one-equation model for ν_T, that represents the lowest level at which a model can be complete. This is designed for aerodynamics applications including boundary layer separation and the equation is:

$$\frac{\overline{D\nu_T}}{\overline{Dt}} = \nabla \cdot \left(\frac{\nu_T}{\sigma_\nu}\nabla \nu_T\right) + S_n u \tag{4.3.6}$$

where S_ν is the source term which depends on the kinematic (ν) and turbulent (ν_T) viscosities, the mean vorticity σ_ν and the turbulent viscosity gradient $\nabla \nu_T$ [15].

4.3.3 Physics Continua Model

In the case of bouyancy driven flows, the **Boussinesq approximation** provides accurate solutions for many thermal convection problems. The model is based on the hypothesis that density differences are sufficiently small and, consequently, the buoyancy forces can be introduced in the momentum equation [16].

Considering an incompressible flow, from the continuity equation it obtains:

$$\overline{\nabla} \cdot \overline{V} = 0 \tag{4.3.7}$$

substituting 4.3.7 in the momentum one, we obtain:

$$\frac{\partial \overline{V}}{\partial t} + \left(\overline{V} \cdot \overline{\nabla}\right)\overline{V} = -\frac{1}{\rho_0}\overline{\nabla p} + \nu \overline{\nabla}^2 \overline{V} + \frac{1}{\rho_0}\overline{F} \tag{4.3.8}$$

where ρ_0 and ρ are, respectively, the reference and local density and $\overline{F} = (\rho - \rho_0)\,\overline{g}$ is the sum of body forces, in this case gravity. Due to the aforementioned hypothesis, it is possible to express it as linear function of temperature:

$$\rho = \rho_0 - \beta \rho_0 \Delta T \tag{4.3.9}$$

where T_0 is reference temperature and β is the *Coefficient of Thermal Expansion*. In this way the momentum equation becomes as follows:

$$\frac{\partial \overline{V}}{\partial t} + \left(\overline{V} \cdot \overline{\nabla}\right) \overline{V} = -\frac{1}{\rho}\overline{\nabla p} + \nu \nabla^2 \overline{V} - \beta \Delta T \overline{g} \tag{4.3.10}$$

To complete the system, it is necessary to consider the energy equation that could be expressed as following:

$$\frac{\partial T}{\partial t} + \overline{u} \cdot \overline{\nabla T} = k \nabla^2 T + \frac{J}{\rho_0 C_p} \tag{4.3.11}$$

where J is the rate per unit volume of internal heat production, k is the thermal diffusivity and $\rho_0 C_p$ is the specific heat capacity per unit volume [17].

4.3.4 Solver Setting

In order to find the right compromise between the physics and the computational cost, several solver setting have been investigated.

In AcuSolve it is possible to set many parameters. In this study, just a few has been deepened starting from the description of the problem:

- **Analisys type**, it allows to decide to set steady or transient simulation;
- **Temperature equation**, it allows to activate energy equation;

- **Turbulence model**, it allows to choose the turbulence model needed.

After that, solver setting follows:

- **Max time step**, it allows to decide the maximum number of iteration if steady state simulation or the physical time step if transient. Each step implements several automatic *Stagger iterations*;
- **Initial time increment**, it allows to set the value of the time step in transient simulation while in steady state is equal to 1e10 because it represents a condition of infinity time;
- **Physical time**, it allows to decide the physical time to investigate;
- **Convergence tolerance**, it allows to decide to stop the simulation when the residuals are under this value;
- **Relaxation factor**, it allows to decide the percentage of the solution to use in the next iteration and this value is applied on all variables;
- **Temperature**, is on when the Temperature equation is activated;
- **Temperature flow**, if is on it uses the coupled Navier-Stokes equations;
- **Turbulence**, it is on when the Turbulence model is activated.

The first set-up tested in the simulation was the Steady State which is showed in tab. 4.4 and 4.5:

Table 4.4: Steady State Problem description

Problem description	**Value**
Analysis type	Steady State
Temperature equation	Advective Diffusive
Turbulence model	Spalart-Allmaras

Table 4.5: Steady-State Solver setting

Solver setting	Value
Max time step	150
Initial time increment (sec)	1e10
Physical time (sec)	-
Convergence tolerance	0.001
Relaxation factor	0.3
Temperature	on
Temperature flow	on
Turbulence	on

The previous set-up showed a certain sensibility to the mesh and boundary conditions; indeed if the mesh is too much refined, the solver detects the smallest vortices inducing instability in the resolution while if it is too much rough, it is possible to generate instability because the problem physics is not detected.

Consequently, to detach to mesh sensitivity, a Transient simulation has been implemented with the following parameters:

Table 4.6: Transient Problem description

Problem description	Value
Analysis type	Transient
Temperature equation	Advective Diffusive
Turbulence model	Spalart-Allmaras

Table 4.7: Transient Solver setting

Solver setting	Value
Max time step	150
Initial time increment (sec)	0.1
Physical time (sec)	10
Convergence tolerance	0.001
Relaxation factor	0.3
Temperature	on
Temperature flow	on
Turbulence	on

In this case, the convergence, as expected, has been reached in an easier way in terms of mesh but the computational time has been raised, therefore this set-up has been excluded and more time has been invested to figure out the right mesh in order to use the *Steady-State Simulation*.

Chapter 5

Base Model Preliminary Analysis

To analyse in detail the thermal-aerodynamics field inside the hypercar front underhood, it is necessary to study the complete model [Fig.5.1] with all the main components and obstacles.

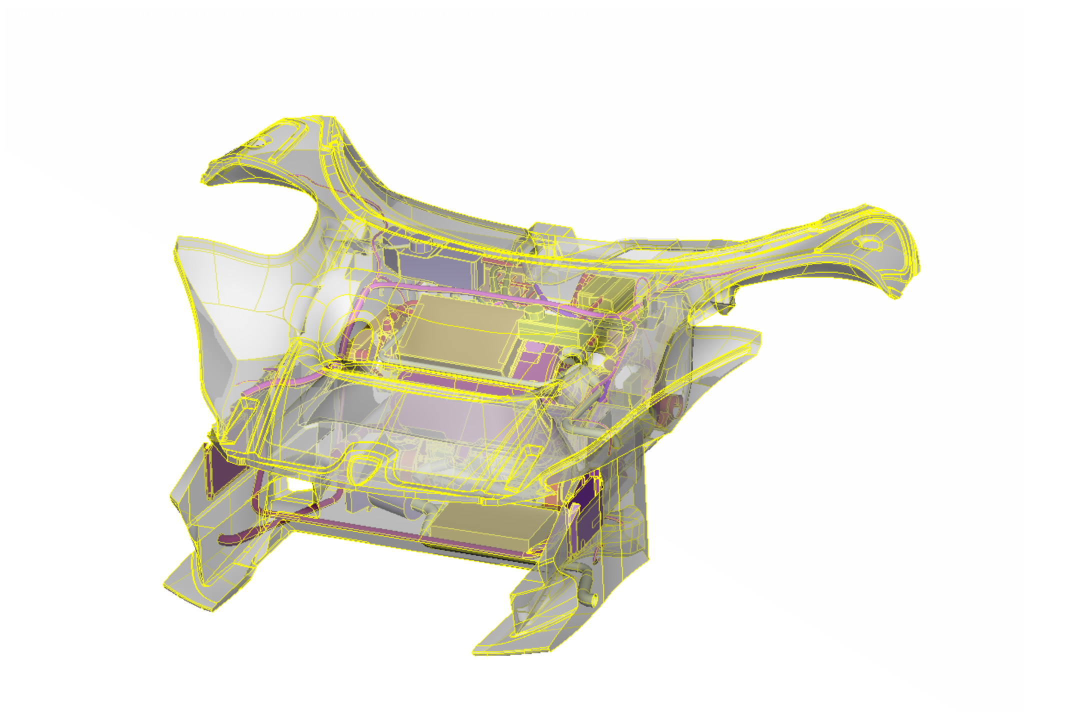

Figure 5.1: C_Two front underhood.

Applying the first step of the methodology described in the previous chapter, the model is composed by the the elements showed in figure 5.2

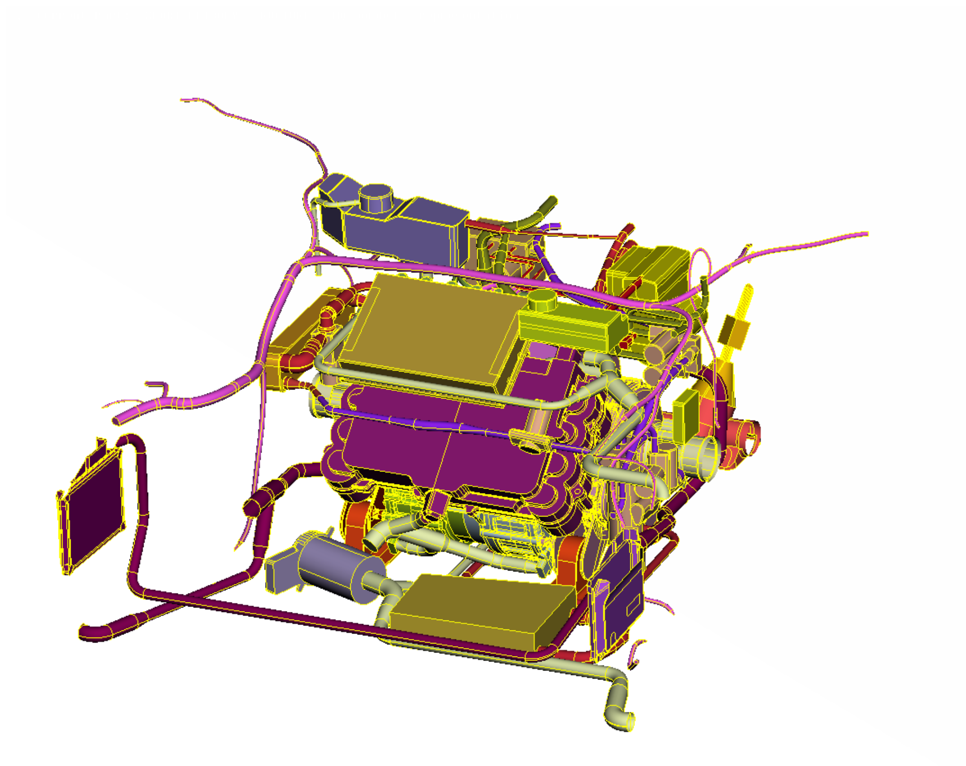

Figure 5.2: Front underhood components.

where the following components are:

- **ABS and brake system - units**;
- **Brake system tubes**;
- **Cabin heat exchanger**;
- **Connectors**;
- **Cooling tank**;
- **Drive-shaft**;
- **ECU units**;
- **Electric power steering pump**;

- **Electrical wirings**;
- **Fittings**;
- **Gearboxes and mounts**;
- **HVAC AC compressor**;
- **Front inverter**;
- **Motors**;
- **PDM unit**;
- **Powertrain battery cooling tubes**;
- **Powertrain cabin heating coolant tubes**;
- **Powertrain refrigerant tubes**;
- **Powertrain front cooling tubes**;
- **PTC heater**;
- **Steering system**;
- **TPMS sensor**;
- **Water pump**.

The investigation has been led imposing the maximum temperature on each element in the worst scenario, that is the track one, understanding if the average value is, globally, under or over the target $T_{ref,glob}$ except in proximity of gearboxes and motors where a $T_{ref,loc}$ higher than 40 % of $T_{ref,glob}$ is accepted.

The components temperatures have been assigned considering the data given by Rimac divisions as showed in tab. 5.1:

Table 5.1: Temperature table.

Front components	**Temperature**
ABS and brake system - unit 1	1.6 $T_{ref,glob}$
ABS and brake system - unit 2	1.2 $T_{ref,glob}$
ABS and brake system - unit 3	1.6 $T_{ref,glob}$
Brake system tubes	0.6 $T_{ref,glob}$
Cabin heat exchanger	0.8 $T_{ref,glob}$
Connectors	1.2 $T_{ref,glob}$
Cooling tank	0.8 $T_{ref,glob}$
Drive-shaft	Adiabatic wall
ECU units	0.8 $T_{ref,glob}$
Electric power steering pump	1.4 $T_{ref,glob}$
Electric HV wiring	1.2 $T_{ref,glob}$
Electric LV wiring	Adiabatic wall
Fittings	Adiabatic wall
Gearboxes	1.7 $T_{ref,glob}$
Gearboxes mounts	Adiabatic wall
HVAC AC compressor	1.2 $T_{ref,glob}$
Front inverter	1.4 $T_{ref,glob}$
Motors	1.6 $T_{ref,glob}$
PDM unit	1.7 $T_{ref,glob}$
Powertrain battery cooling tubes	0.8 $T_{ref,glob}$
Powertrain cabin heating cooling tubes	0.8 $T_{ref,glob}$
Powertrain cabin refrigerant tubes	0.8 $T_{ref,glob}$
Powertrain front cooling tubes	0.8 $T_{ref,glob}$
PTC heater	Adiabatic wall
Steering column	Adiabatic wall
Steering rack	Adiabatic wall
TPMS sensor	Adiabatic wall
Water pump	1.4 $T_{ref,glob}$

The base model has five openings: one on top, two on side extrusions and two inside the wheel-arches. In order to determine which of them are inlets or outlets, several test cases with different boundary conditions have been performed in the next sections.

5.1 First test case

The first test case has been set referring to the boundary conditions applied by Rimac in a simulation with the compartment version described in section 4.3.

Table 5.2: Boundary conditions of first test case.

Left and Right Inlets	**Value**
Mass flow rate	$\dot{m}_{ref}$
Temperature	0.5 $T_{ref,glob}$
Outlet	**Value**
Static Pressure $[Pa]$	0
Wheel-arches Walls	**Value**
Heat Transfer Coefficient $[\frac{W}{m^2K}]$	0.5 $T_{ref,glob}$
Ambient Temperature	0.5 $T_{ref,glob}$
Compartment walls	**Value**
Heat Transfer Coefficient $[\frac{W}{m^2K}]$	10
Ambient Temperature	0.5 $T_{ref,glob}$

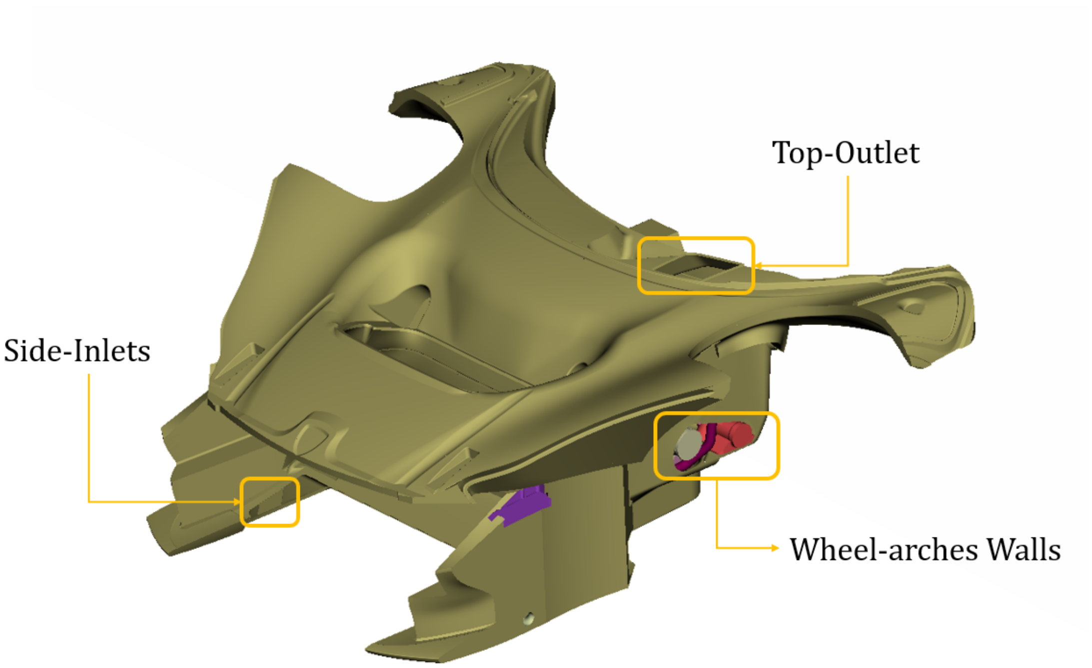

Figure 5.3: Inlets and outlet of the first test case.

This simulation run aims to verify that the aforementioned methodology works properly with a more complex geometry. These boundary conditions do not represent the real ones due to the fact that wheel-arches are, actually, open and the top outlet is located close to a zone which is at high pressure. These reasons led to investigate deeply the right values of the boundary conditions.

5.2 Second test case

5.2.1 External Aerodynamics Model

In order to extrapolate more realistic values, an external aerodynamic simulation of a closed baseline car [Fig.5.4] has been performed.

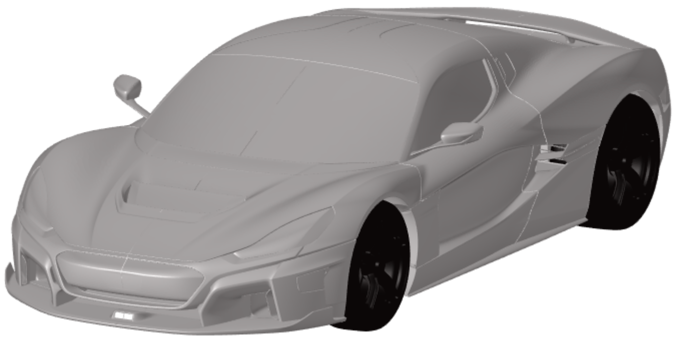

(a) *Isometric view*

(b) *Side view*

Figure 5.4: Rimac C_Two CFD model.

To simplify the model, some components have not been simulated [Fig. 5.5]:

- MRF for wheels;
- Suspension assembly;
- Brake assembly;
- Radiators.

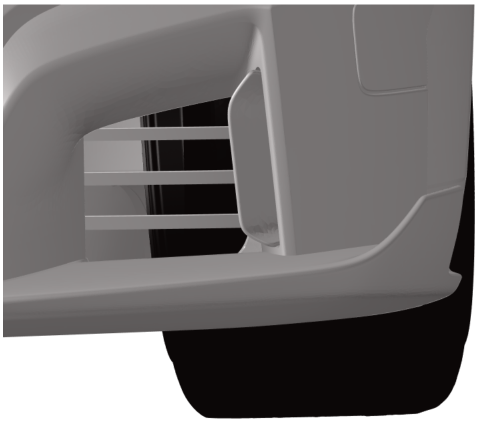

(a) *Front airduct*

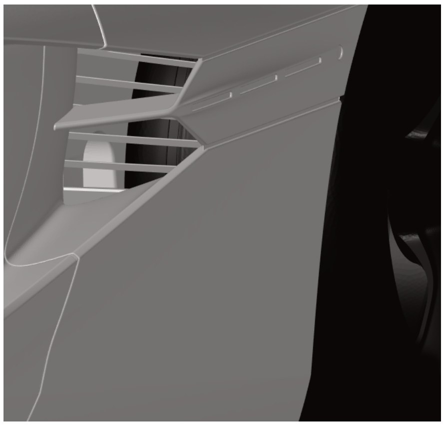

(b) *Rear airduct*

Figure 5.5: Rimac C_Two CFD model details.

The problem has been set with the following parameters:

Table 5.3: External aerodynamics setting.

Problem description	**Value**
Analysis type	Staedy State
Turbulence model	Spalart-Allmaras
Iterations	150

Table 5.4: External aerodynamics boundary conditions.

BC	**Value**
Velocity Inlet	150 kph
Pressure Outlet	0 Pa
Wheels rotation speed	117.4 rad/s

The pressure coefficient distribution, showed in fig. 5.6, on the car body is quite similar to expected.

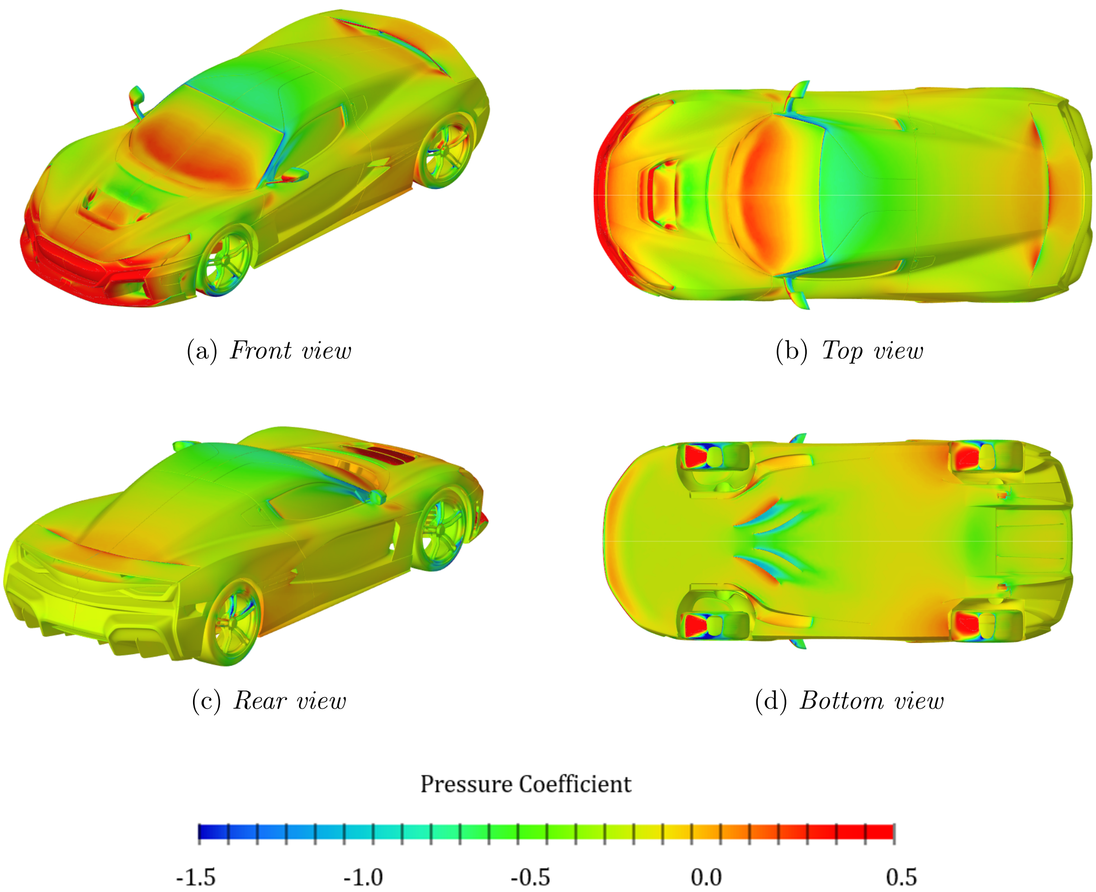

(a) *Front view* (b) *Top view*

(c) *Rear view* (d) *Bottom view*

(e) *Cp scale*

Figure 5.6: Cp field on Rimac C_Two

In the figures, an important characteristic to analyse in order to understand if the solution is physically correct, is the respect of pressure field on A-pillar which is verified. It is also possible to note the high pressure zone under the splitter, this is due to the different ride height of this model with respect to the real CFD model used to evaluate the aerodynamic performance of the car. Moreover, the solution shows the low pressure on the roof of the car, immediately after the windscreen, where the airflow accelerates to follow the curvature and the pressure recovery due to the presence of the rear wing as well. On the underbody, it is possible to understand the power of vortex generators in order to create extreme lower pressure in the front zone to increase the downforce. The diffuser, indeed, is able to work in the right way ensuring a good level of vertical force on the rear axle.

5.2.2 Boundary conditions setting

Focusing on the interesting zones, it was possible to extract mean values of pressure to use as new boundary conditions:

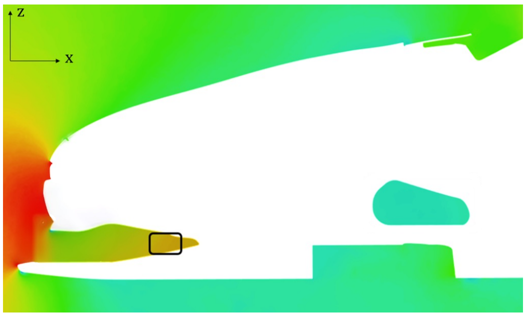

(a) *Side-Outlets view*

(b) *Wheel-arches Inlets view*

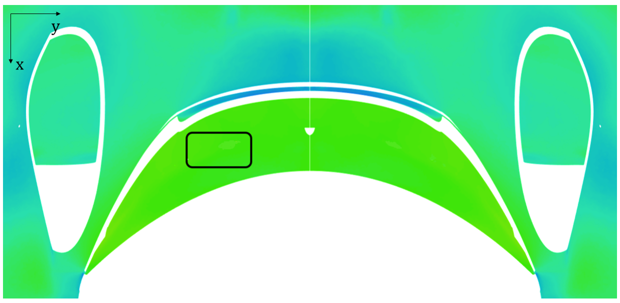

(c) *Top-Inlet view*

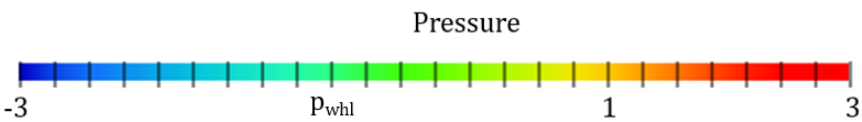

(d) *Pressure scale referred to wheel-arches pressure*

Figure 5.7: Pressure field on Inlets and Outlets

From these scenes, it has been possible to note as the previous outlet seems to behave as inlet and wheel-arches as outlets.

Table 5.5: Boundary conditions of second test case.

Left and Right Inlets	**Value**
Total Pressure	p_{ref}
Temperature	$0.5\ T_{ref,glob}$
Top Inlet	**Value**
Total Pressure	p_{ref}
Temperature	$0.5\ T_{ref,glob}$
Wheel-arches Outlets	**Value**
Static Pressure	$0.99\ p_{ref}$
Compartment walls	**Value**
Heat Transfer Coefficient $\left[\frac{W}{m^2 K}\right]$	10
Ambient Temperature	$0.5\ T_{ref,glob}$

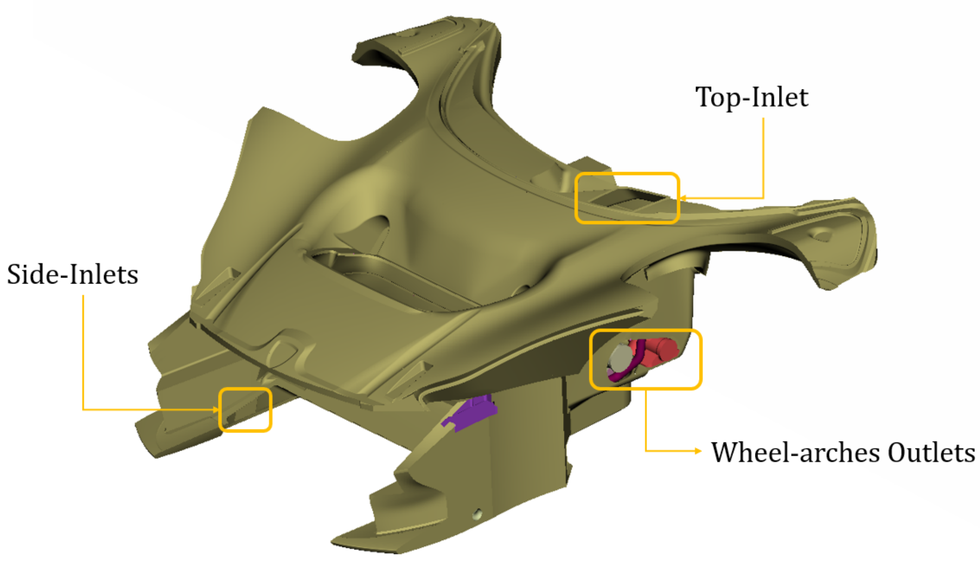

Figure 5.8: Inlets and outlet of the second test case.

The reason of this inversion of conditions is due to the fact that there are not any holes in the chassis. Consequently, in the zone of top-inlet a recirculation bubble is generated increasing locally the pressure as along the side-outlets while the wheel-arches are ever disturbed by vortices created by the wheels.

5.3 Third test case

5.3.1 First Half of Car Model

It was clear that even the external aerodynamics of a closed car has not been useful to determine the real boundary conditions. An aerodynamics simulation of the C_Two front half has been performed, including the compartment without imposing any temperatures, as showed in figure:

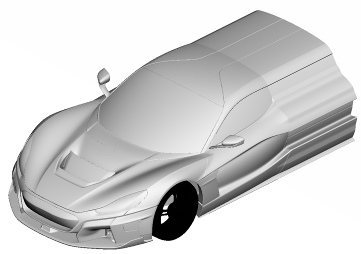

Figure 5.9: Front section car of Rimac C_Two.

This choice has been taken to reduce the computational cost but, to avoid the influence of pressure outlet due to its closeness to the compartment, the car body was lengthened by 1 meter as in figures:

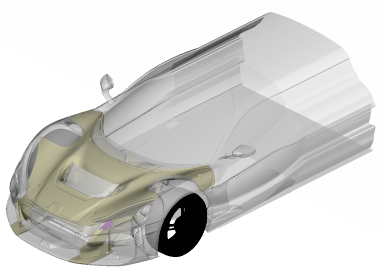

(a) *Compartment inside front half car*

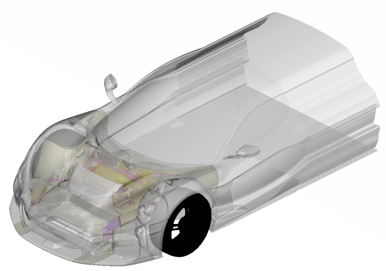

(b) *Components inside front half car*

Figure 5.10: Front section car with the whole compartment

5.3.2 Boundary conditions setting

Focusing on the interesting zones, it was possible to extract mean values of pressure to use as new boundary conditions confirmed by Rimac simulation of the full vehicle with the compartment object of study inside:

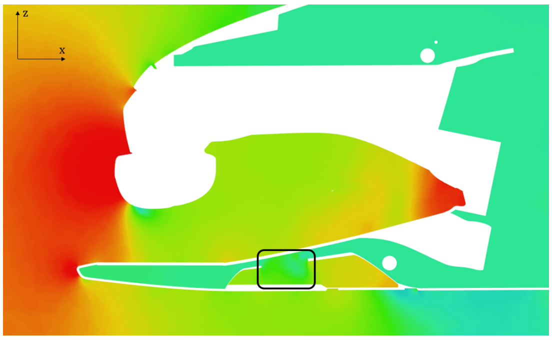

(a) *Side-Inlets view*

(b) *Wheel-arches Outlets view*

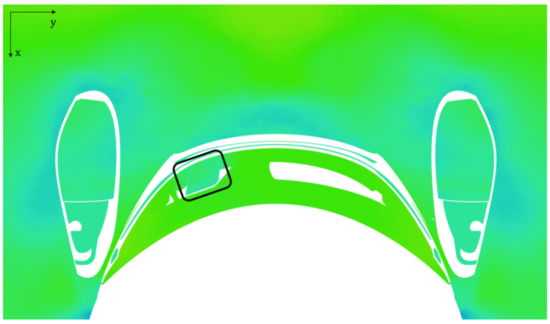

(c) *Top-Inlet view*

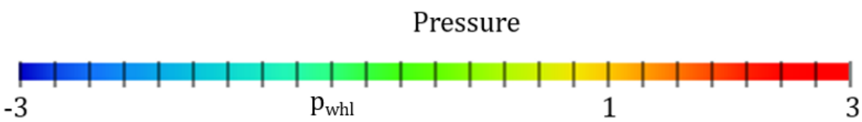

(d) *Pressure scale referred to wheel-arches pressure*

Figure 5.11: Pressure field on Inlets and Outlets

These values confirmed the previous one but they are more realistic than external aerodynamics because in the latter the compartment was not included . For example, in the top inlet area, as aforementioned, the recirculation bubble is always present but with less effect due to wheel-arches suction.

Table 5.6: Boundary conditions of third test case.

Left and Right Inlets	**Value**
Total Pressure	p_{ref}
Temperature	0.5 $T_{ref,glob}$
Top Inlet	**Value**
Total Pressure	p_{ref}
Temperature	0.5 $T_{ref,glob}$
Wheel-arches Outlets	**Value**
Left Static Pressure	0.9987 p_{ref}
Right Static Pressure	0.9986 p_{ref}
Compartment walls	**Value**
Heat Transfer Coefficient $\left[\frac{W}{m^2K}\right]$	10
Ambient Temperature	0.5 $T_{ref,glob}$

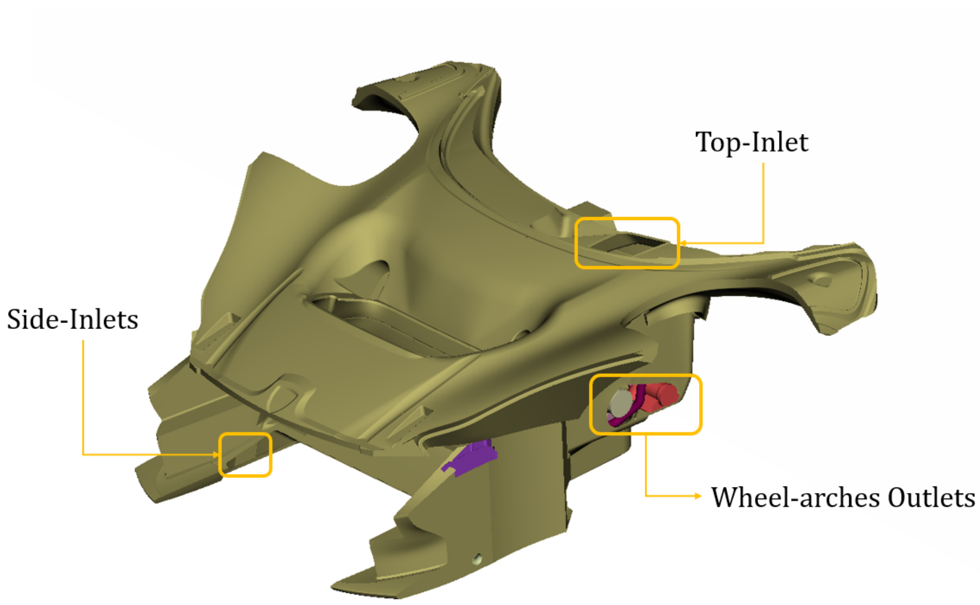

Figure 5.12: Inlets and outlet of the third compartment model.

Chapter 6

Results

6.1 Base Model

Downstream the previous considerations, a simulation of the base model has been performed to understand how airflow is inside the compartment.

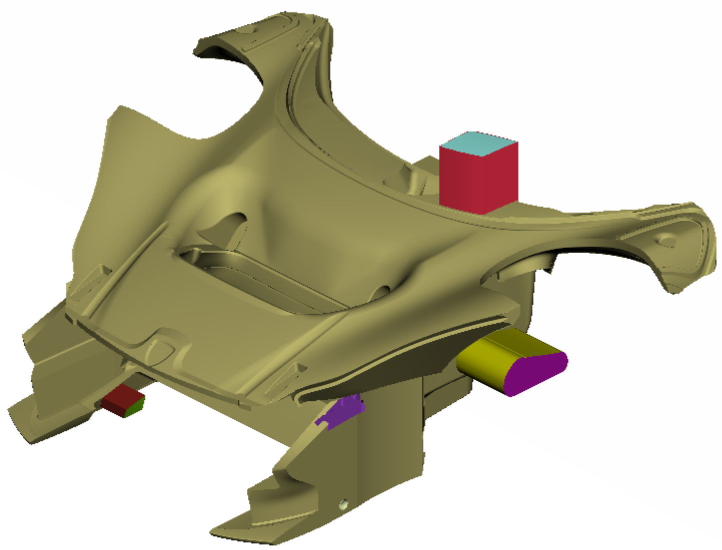

Figure 6.1: Base model with plenum.

In order to obtain a robust and realistic model without simulating the whole car, it has been necessary to add inlets and outlets plenum, as showed in figure 6.1. This technique is often used in many similar cases, as for HVAC (Heating, Ventilation and Air Conditioning) studies [18], to reduce the computational cost respecting always the physics of the problem.

From the following scenes, it has been possible to note as inside the box the average temperature is higher than 20% of $T_{ref,glob}$ [Fig. 6.3]. In particular, in the zones between the gearboxes, motors and inverters, it is higher than 14% of $T_{ref,loc}$ [Fig. 6.5], as showed in figures:

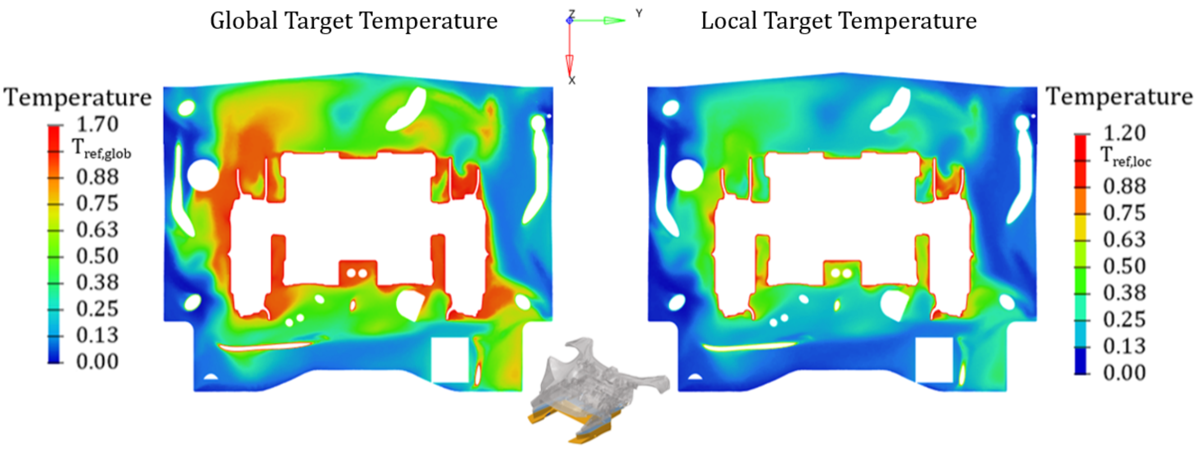

Figure 6.2: Global and Local Target Temperature on Gearboxes and motors XY section.

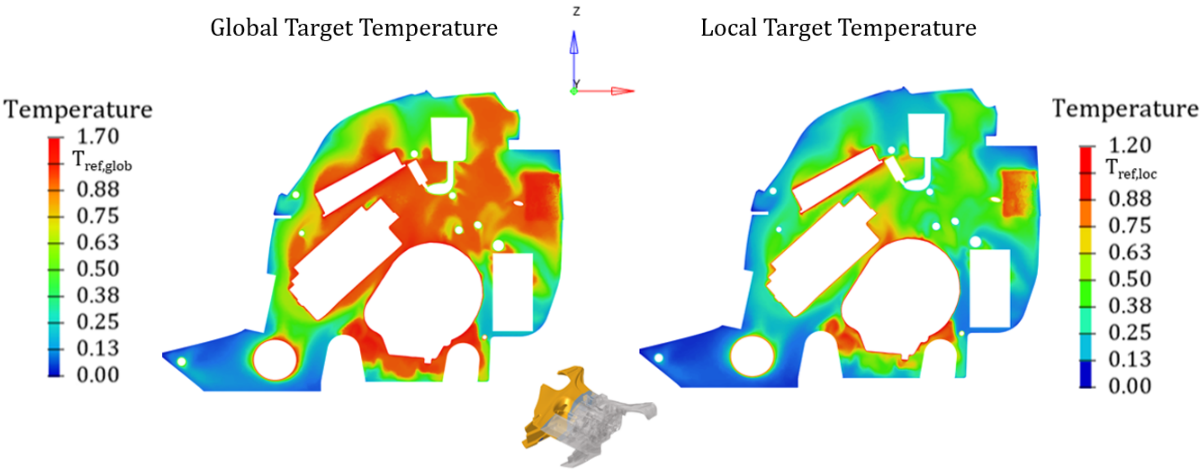

Figure 6.3: Global and Local Target Temperature on Gearboxes and Inverter XZ section.

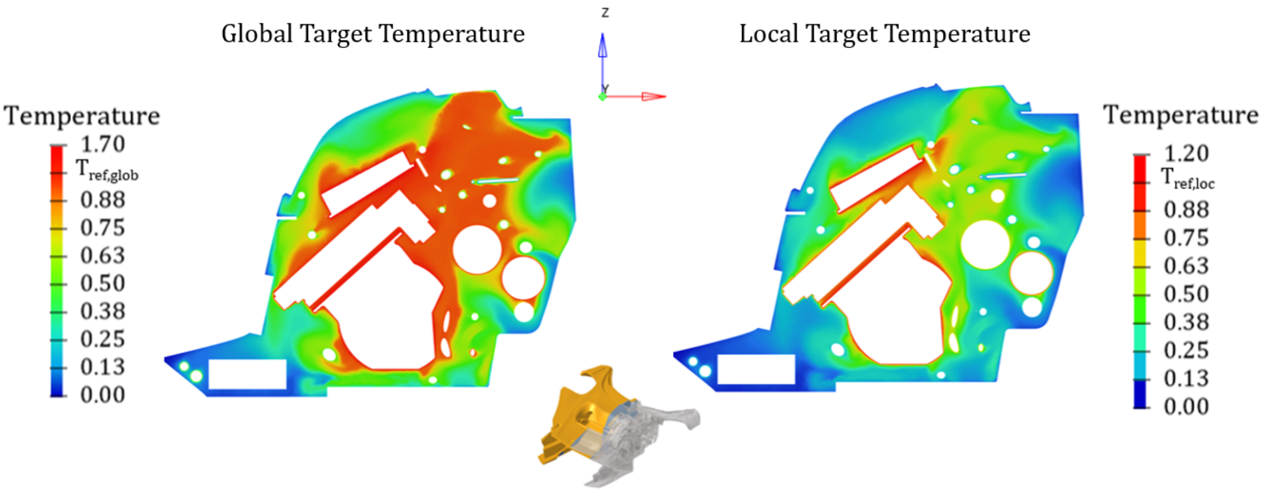

Figure 6.4: Global and Local Target Temperature on Symmetry plane XZ section.

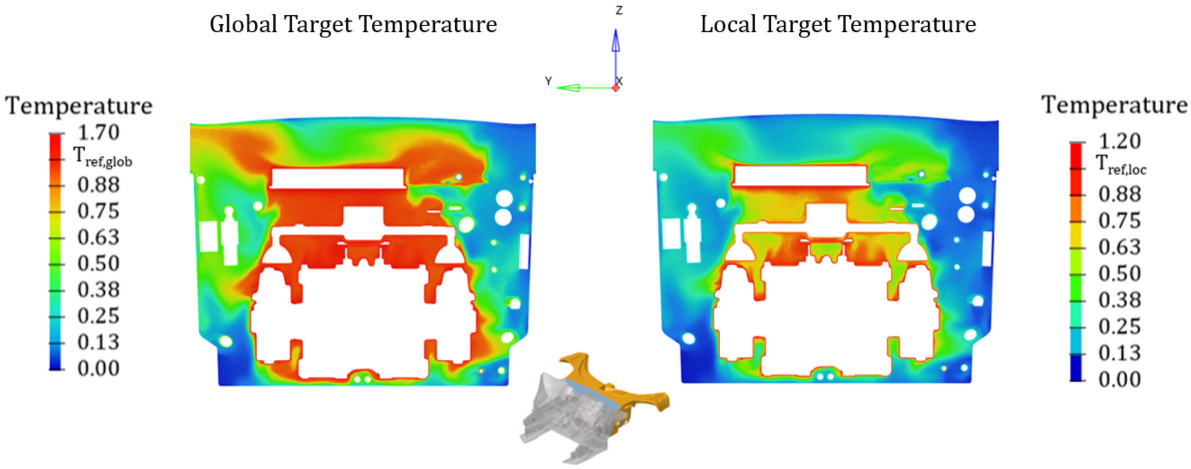

Figure 6.5: Global and Local Target Temperature on Gearboxes, PDM unit and motors YZ section .

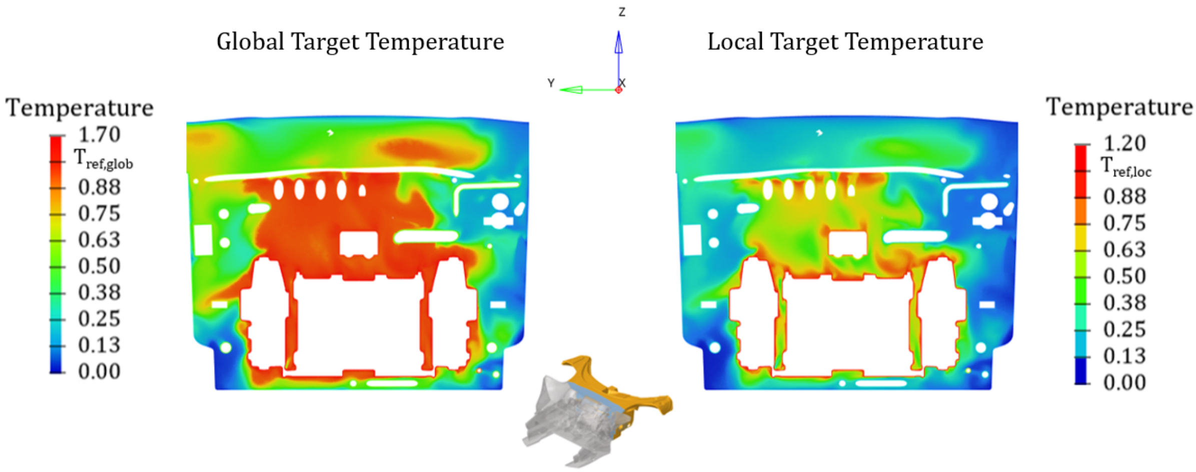

Figure 6.6: Global and Local Target Temperature on Gearboxes, PDM unit and motors YZ section 2.

These high values are due to the low velocities around the elements as showed in figure 6.7; indeed, in this way the flow has not enough kinetic energy to transport away the heat transferred by them.

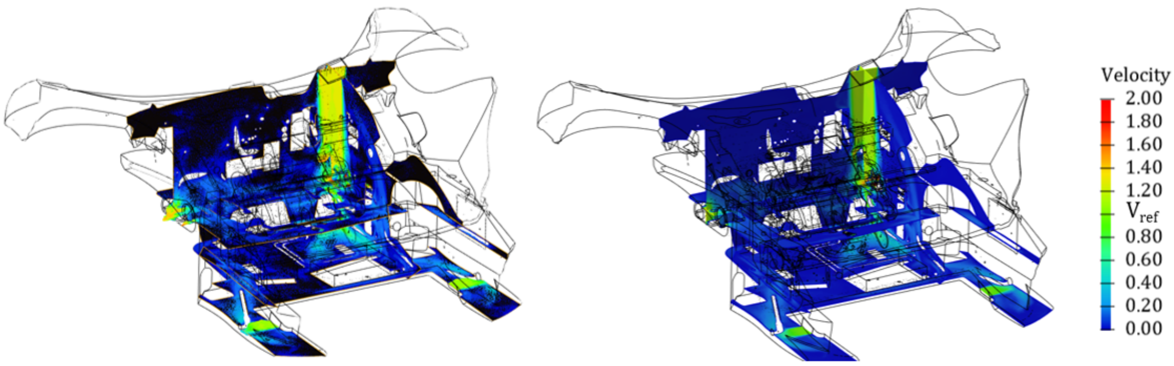

Figure 6.7: Velocity on different sections.

6.2 Optimized Models

As described in the previous paragraph, the temperature field inside the compartment is quite critical despite them being electrical components. According to Rimac Automobili Vehicle Engineering division and AMET CFD, the objective is to identify, after the thermal analysis, the needed mass flow to satisfy the cooling requirements, paying attention to the temperature around the TPMS sensor.

6.2.1 Bottom Inlets

Thinking in this ways, several solutions have been studied. The first one regards the implementation of two symmetric bottom inlets, positioned exactly below the gearboxes between the relative mounts because they are among the most stressed components, as follows:

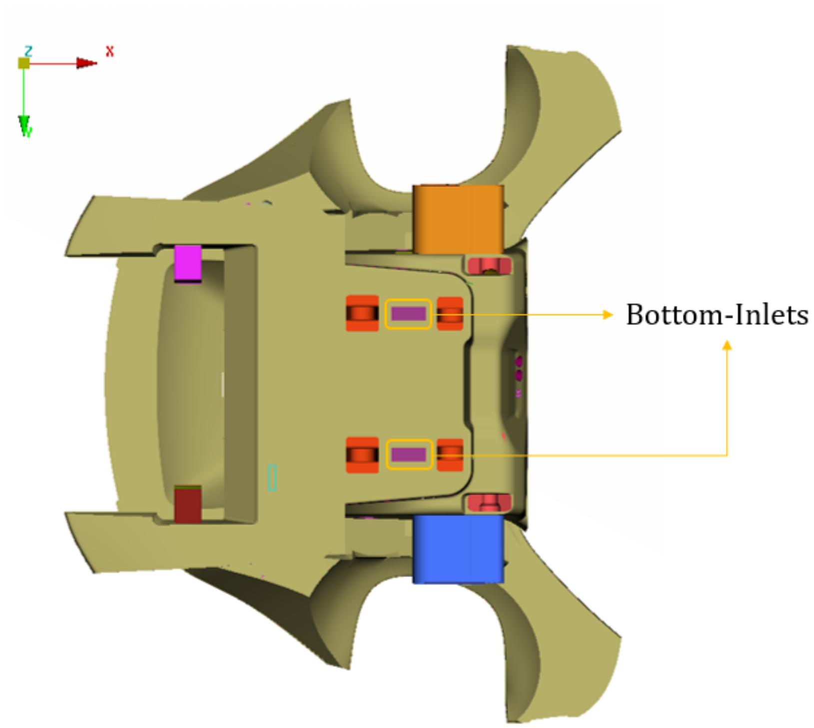

Figure 6.8: Bottom inlets.

They could be realised through appropriate Naca ducts on the car floor as some of the most famous ICE hypercar and for this reason, to achieve the aim, several mass flow rates have been tested:

Table 6.1: Mass flow rates from the bottom inlets.

Mass flow rate	Value
$\dot{m}_{b,1}$	$0.5\ \dot{m}_{ref}$
$\dot{m}_{b,2}$	$1.0\ \dot{m}_{ref}$
$\dot{m}_{b,3}$	$1.5\ \dot{m}_{ref}$
$\dot{m}_{b,4}$	$2.0\ \dot{m}_{ref}$
$\dot{m}_{b,5}$	$2.5\ \dot{m}_{ref}$

After studying the thermal-aerodynamics field, it has been possible to note as over $\dot{m} > \dot{m}_3 = 1.5\dot{m}_{ref}$ the rise of mass flow rate does not bring a decrease of global temperature. The reason is the kinetic energy lost due to the impact on the gearboxes and, in this way, the velocity field obtained around the components is quite similar [Fig. 6.9].

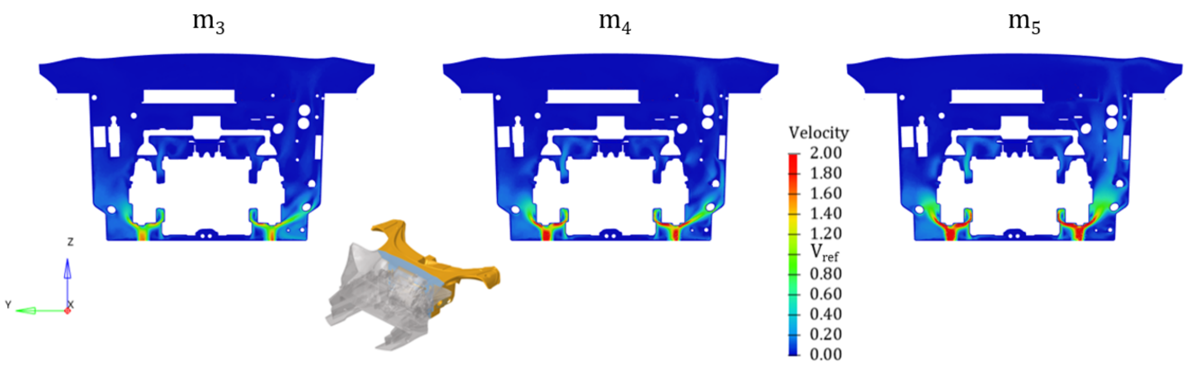

Figure 6.9: Bottom inlets velocities.

The thermal analysis led to figure out as some hot spot has been deleted, as showed in the following figures. Indeed the most critical zones, as gearboxes and motors ones, are wetted by a little bit colder flow coming from the new bottoms inlets which allows to carry out a small quantity of heat through the outlets, in particular the right one. The last observation is explained by the asymmetrical position of components which probably creates a positive canalization of the airflow.

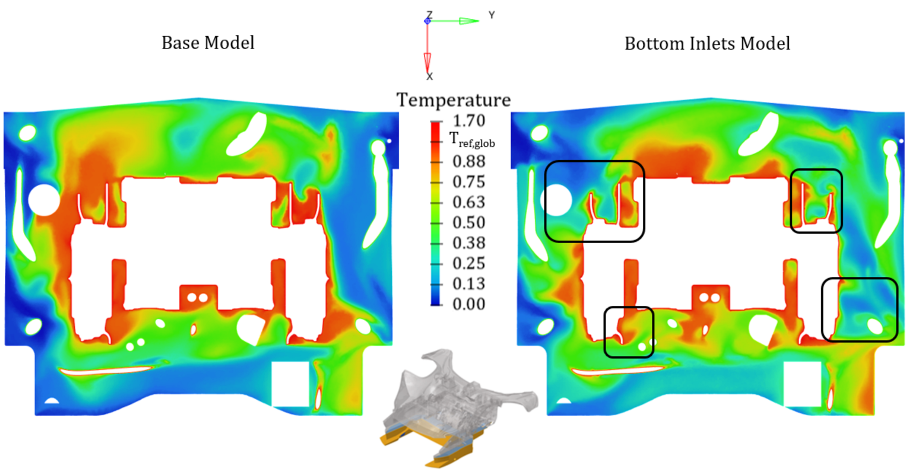

Figure 6.10: Global Target Temperature on Gearboxes and motors XY section.

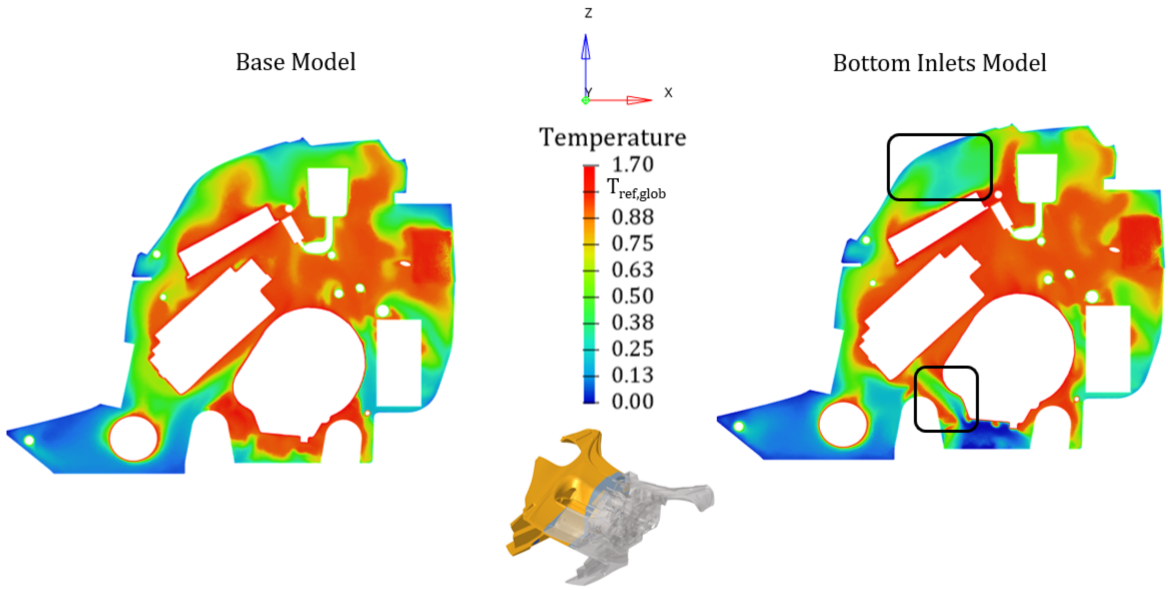

Figure 6.11: Global Target Temperature on Gearboxes and Inverter XZ section.

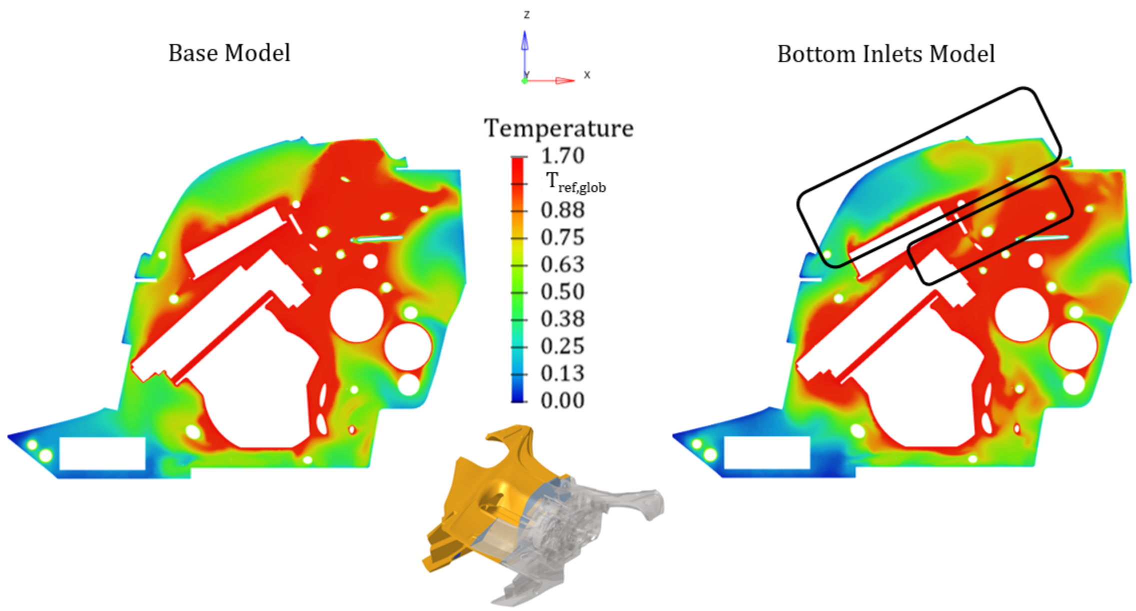

Figure 6.12: Global Target Temperature on Symmetry plane XZ section.

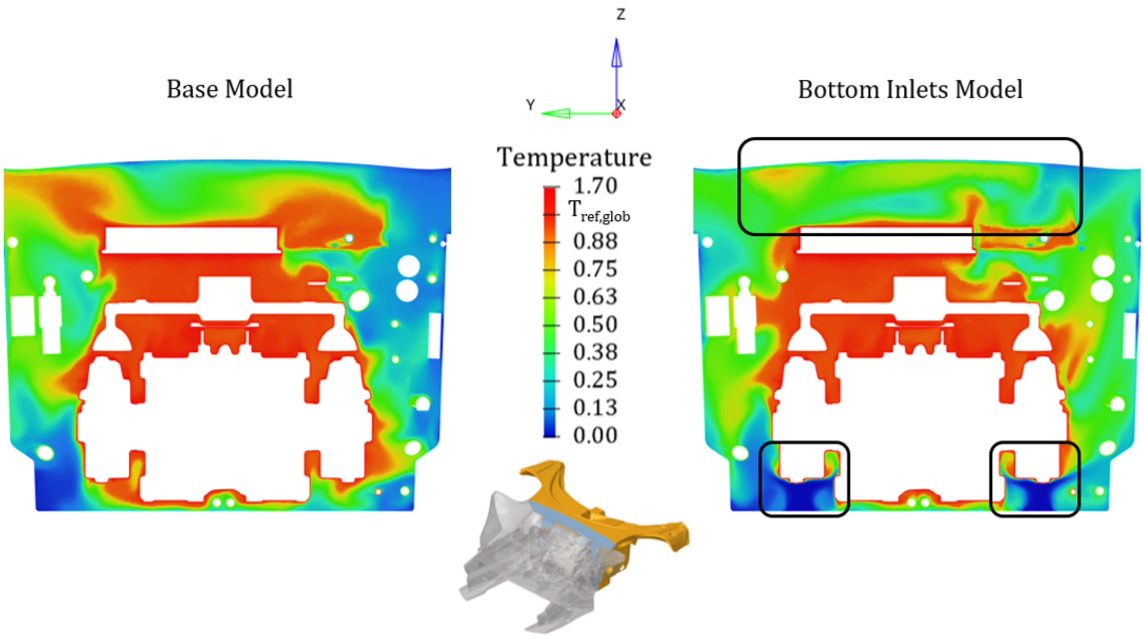

Figure 6.13: Global Target Temperature on Gearboxes, PDM unit and motors YZ section 1.

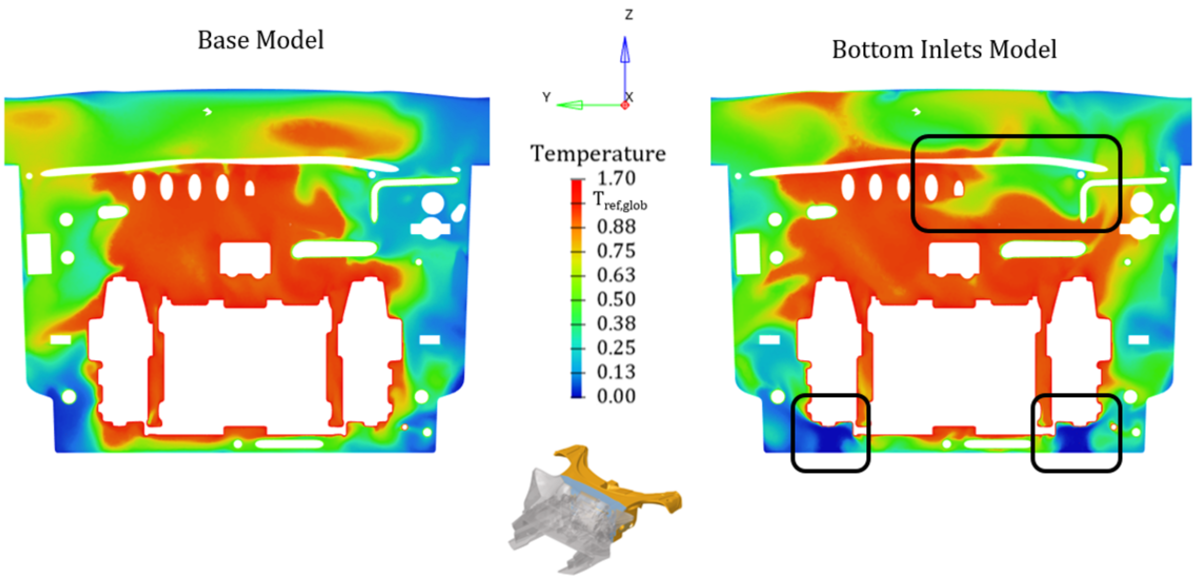

Figure 6.14: Global Target Temperature on Gearboxes, PDM unit and motors YZ section 2.

In the previous scenes it has been noted as around the main components, there is a sensible reduction closing the gap with the $T_{ref,loc}$ as showed in the following figures:

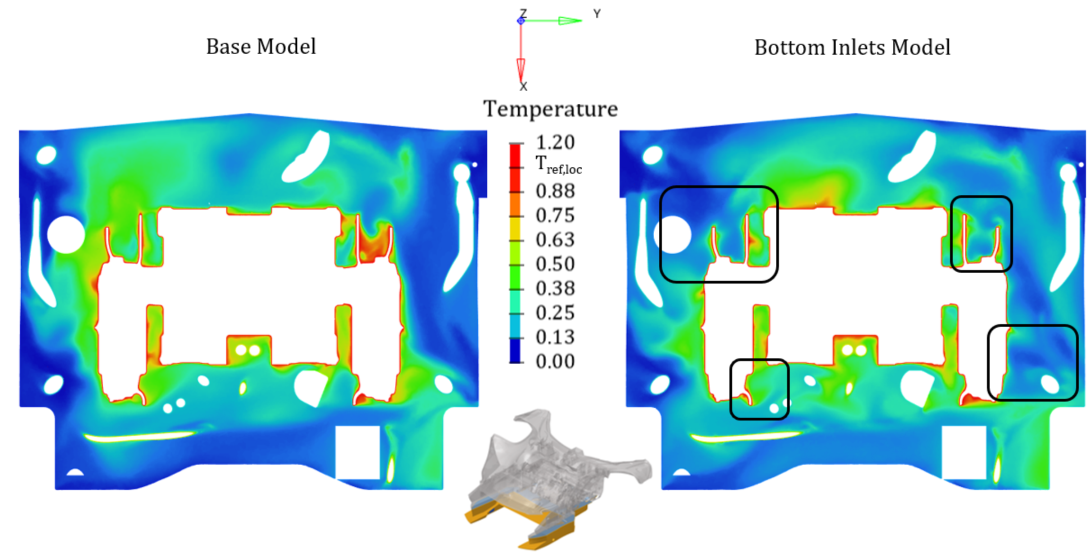

Figure 6.15: Local Target Temperature on Gearboxes and motors XY section.

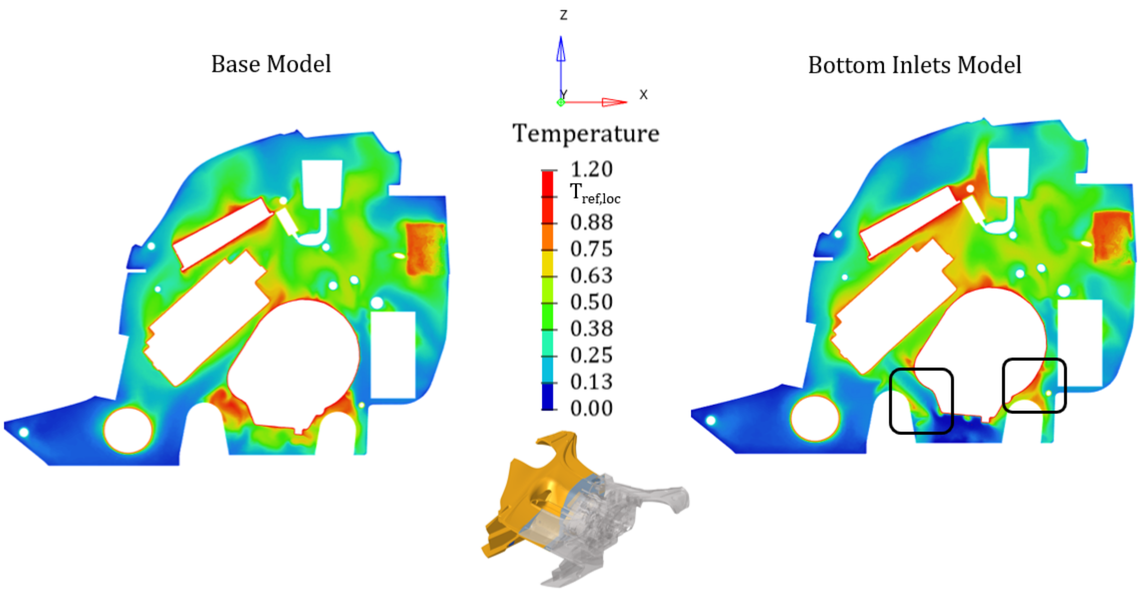

Figure 6.16: Local Target Temperature on Gearboxes and Inverter XZ section.

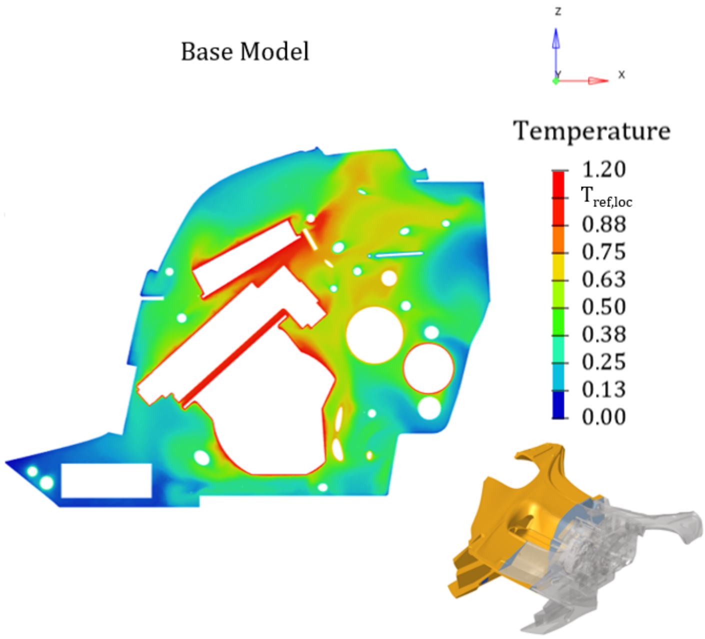

Figure 6.17: Local Target Temperature on Symmetry plane XZ section.

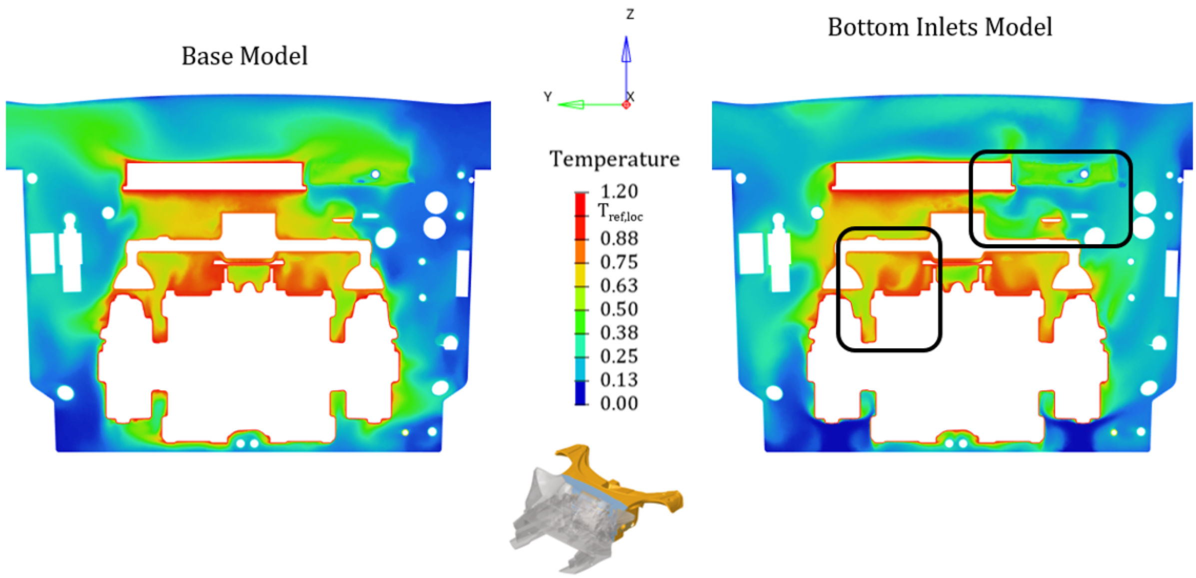

Figure 6.18: Local Target Temperature on Gearboxes, PDM unit and motors YZ section 1.

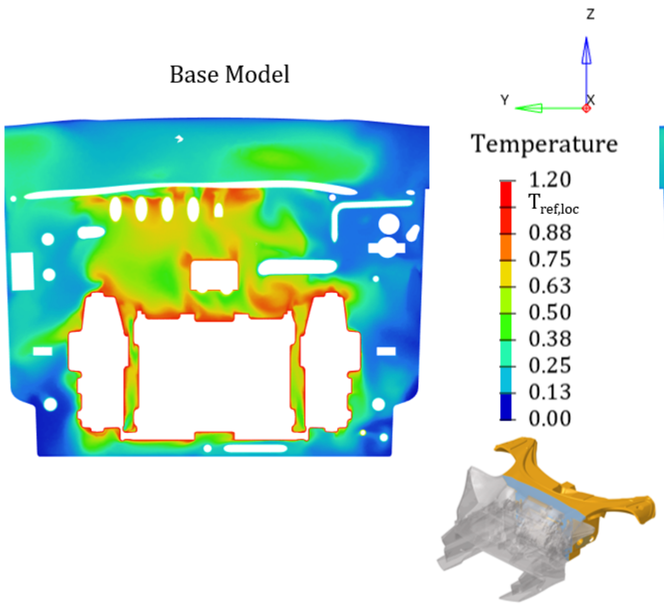

Figure 6.19: Local Target Temperature on Gearboxes, PDM unit and motors YZ section 2.

Despite this improvement, most part of the heat is trapped between the elements because the flows seems to be stopped there, as showed in figure 6.18.

6.2.2 Front Inlet

Due to the limited improvements obtained with the bottom inlets, another solution has been investigated trying to increase the cooling airflow. It has been created a front inlet located in the lower side of the compartment taking an advantage from the high pressure generated by the presence of the front radiators. Due to the lack of them in the simplified model of the car, it has been imposed a reasonable mass flow rate, according to Rimac Aerodynamics division, instead of pressure value.

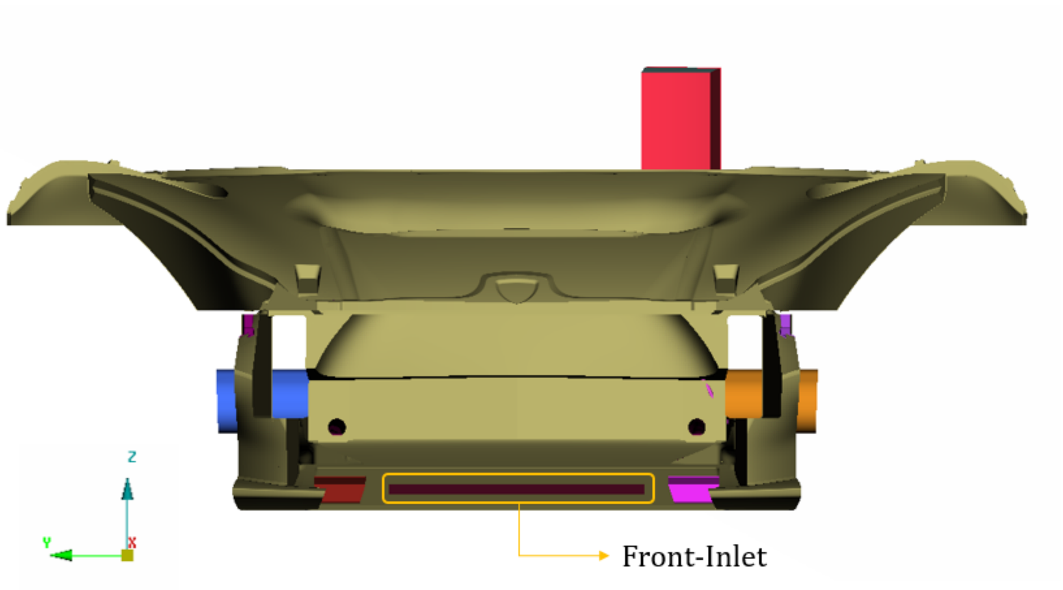

Figure 6.20: Front inlet.

The upper value of the mass flow rate is chosen to prevent a large increase of the drag but also to ensure enough cooling to the front compartment.

Table 6.2: Mass flow rates from the front inlet

Mass flow rate	**Value**
$\dot{m}_{f,1}$	$5.0\ \dot{m}_{ref}$
$\dot{m}_{f,2}$	$7.0\ \dot{m}_{ref}$
$\dot{m}_{f,3}$	$9.0\ \dot{m}_{ref}$

Analysing the aero-thermal field the first value of mass flow has resulted optimal because it brings an effective improvement, as showed in the following figures, but also it could be, actually, implemented according to Rimac Automobili Vehicle Engineering division.

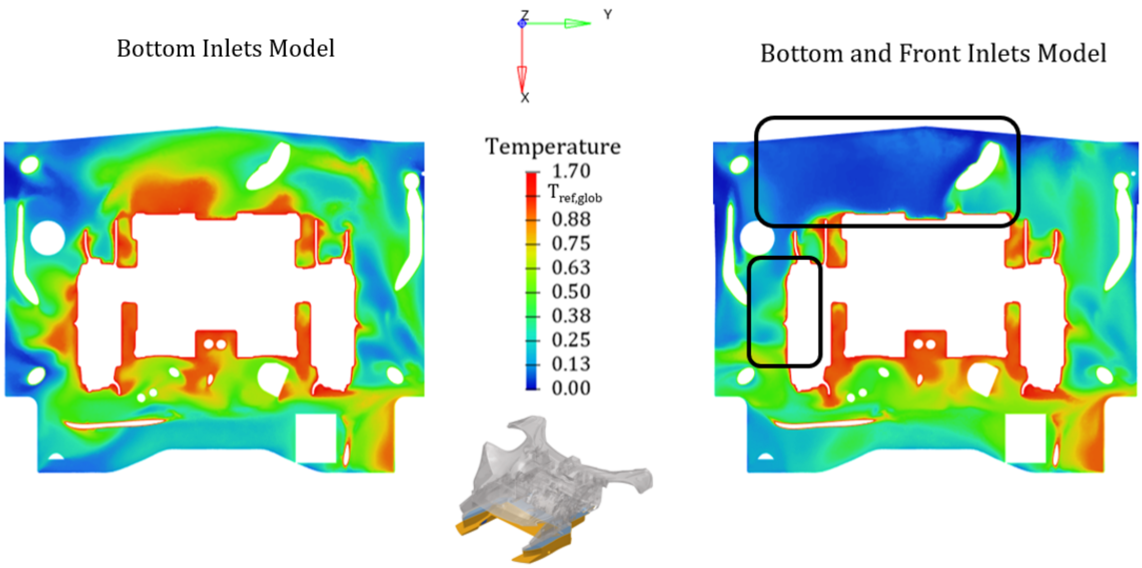

Figure 6.21: Global Target Temperature on Gearboxes and motors XY section.

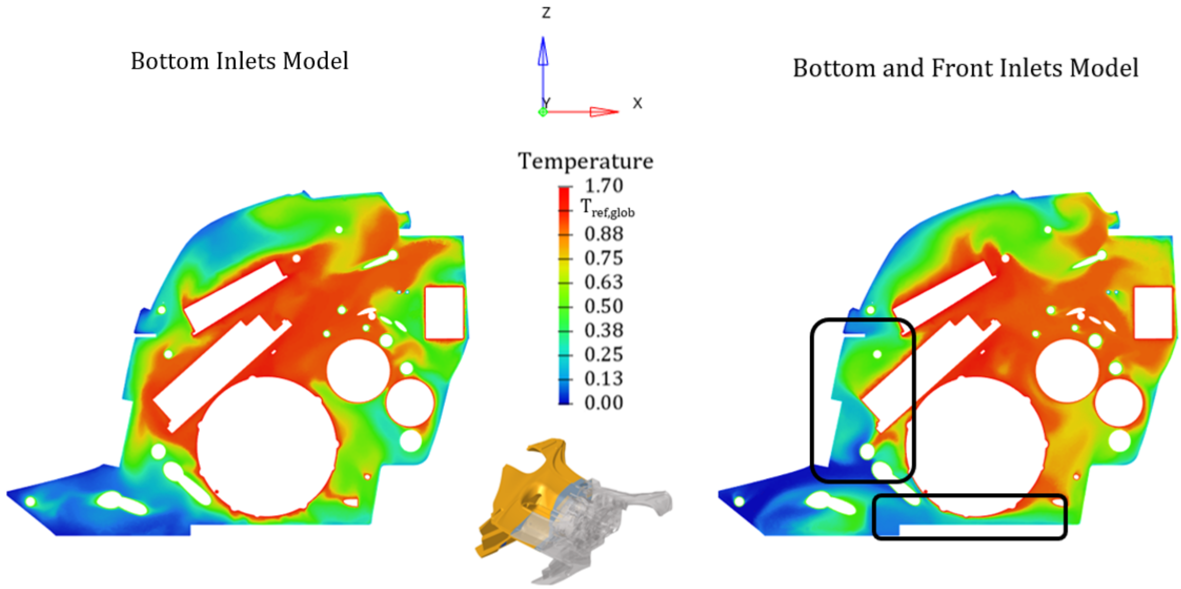

Figure 6.22: Global Target Temperature on Gearboxes and Inverter XZ section.

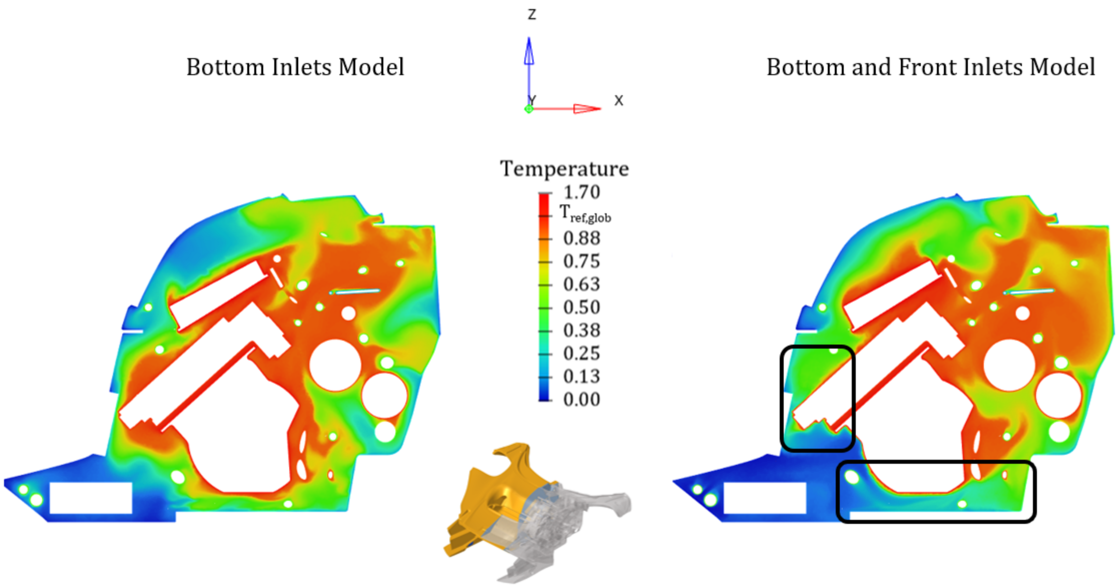

Figure 6.23: Global Target Temperature on Symmetry plane XZ section.

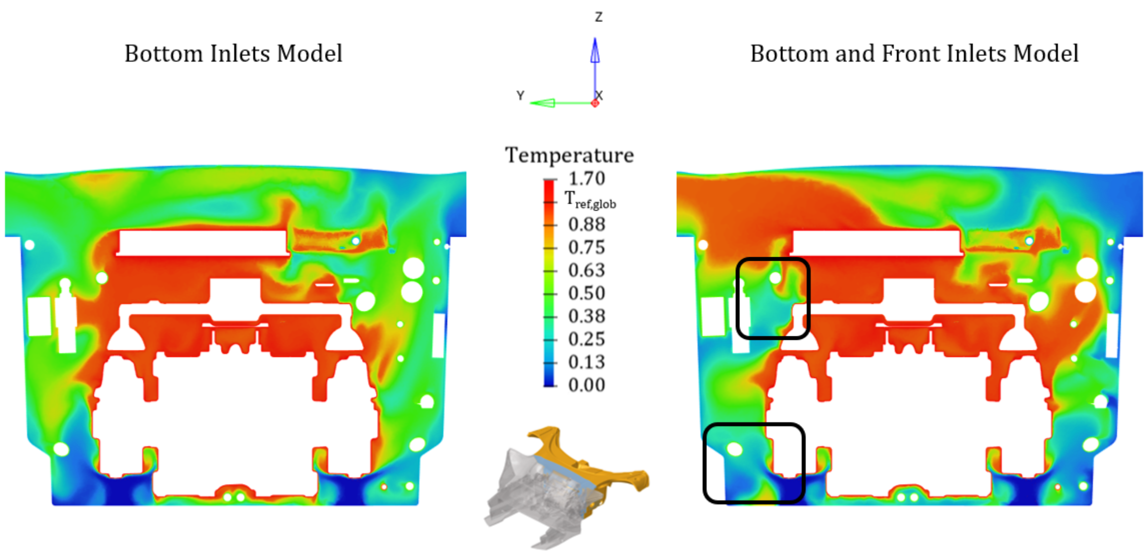

Figure 6.24: Global Target Temperature on Gearboxes, PDM unit and motors YZ section 1.

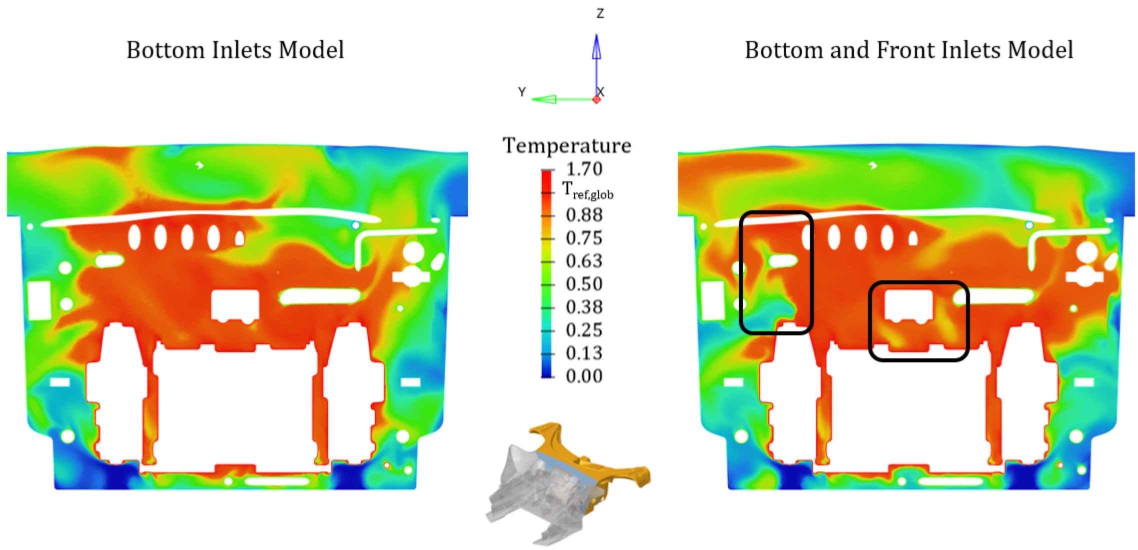

Figure 6.25: Global Target Temperature on Gearboxes, PDM unit and motors YZ section 2.

The front inlet moved the heated air to the back of compartment but the critical zones are cooled ensuring the performance during the worst scenario, as it is possible to see in the following figures.

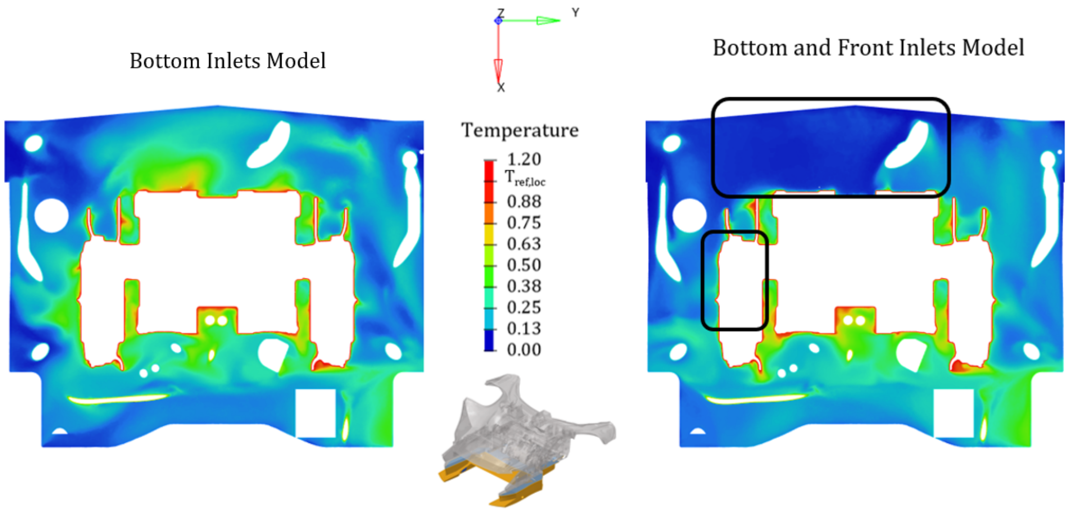

Figure 6.26: Local Target Temperature on Gearboxes and motors XY section.

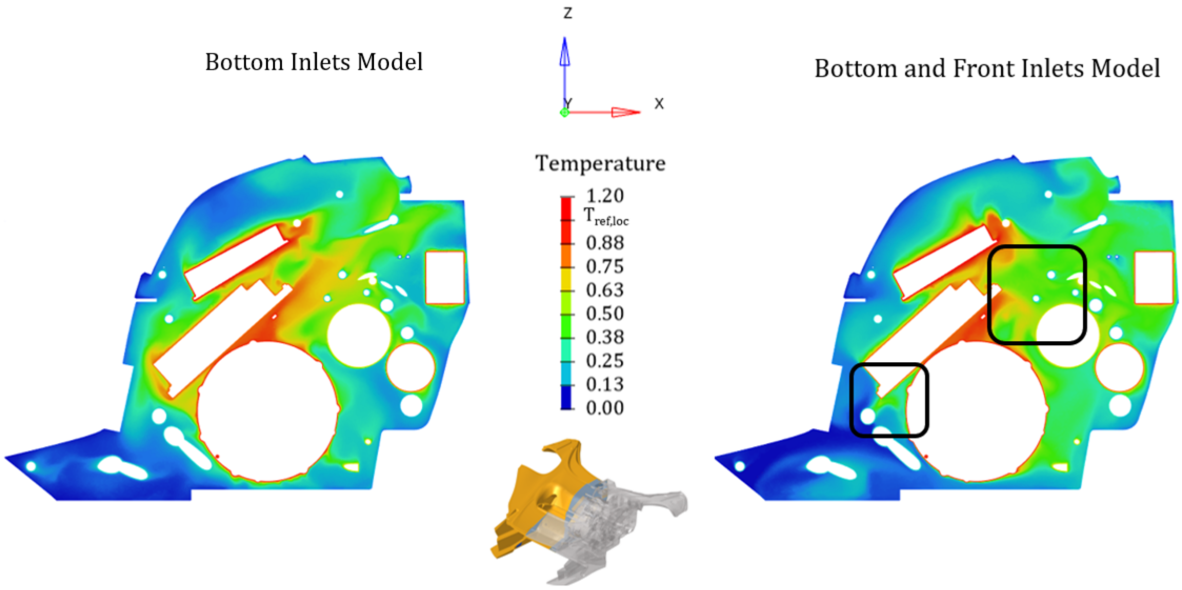

Figure 6.27: Local Target Temperature on Gearboxes and Inverter XZ section.

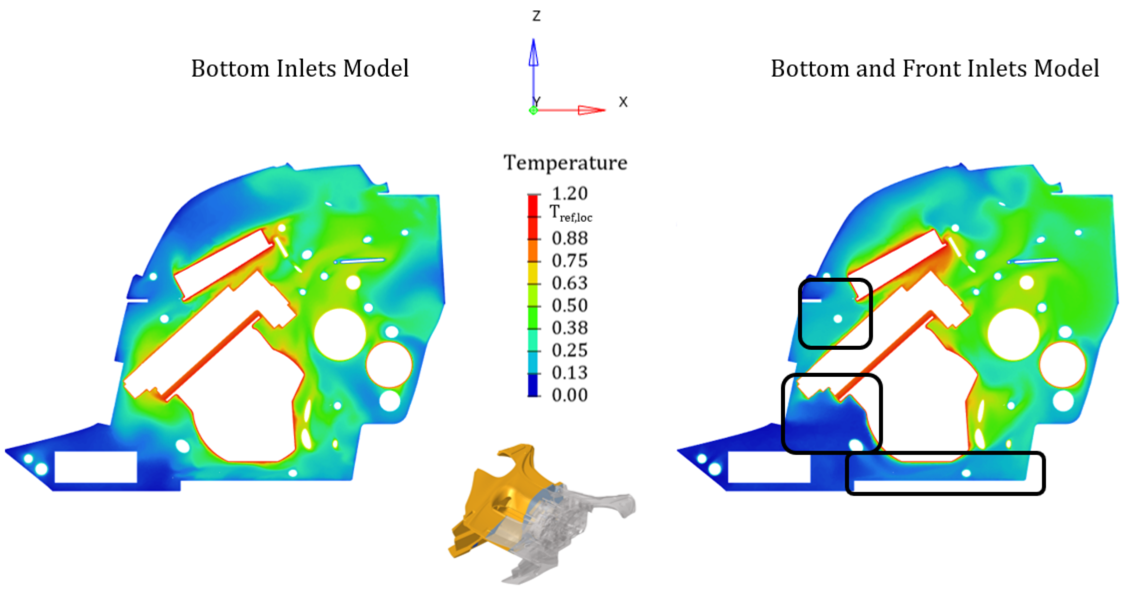

Figure 6.28: Local Target Temperature on Symmetry plane XZ section.

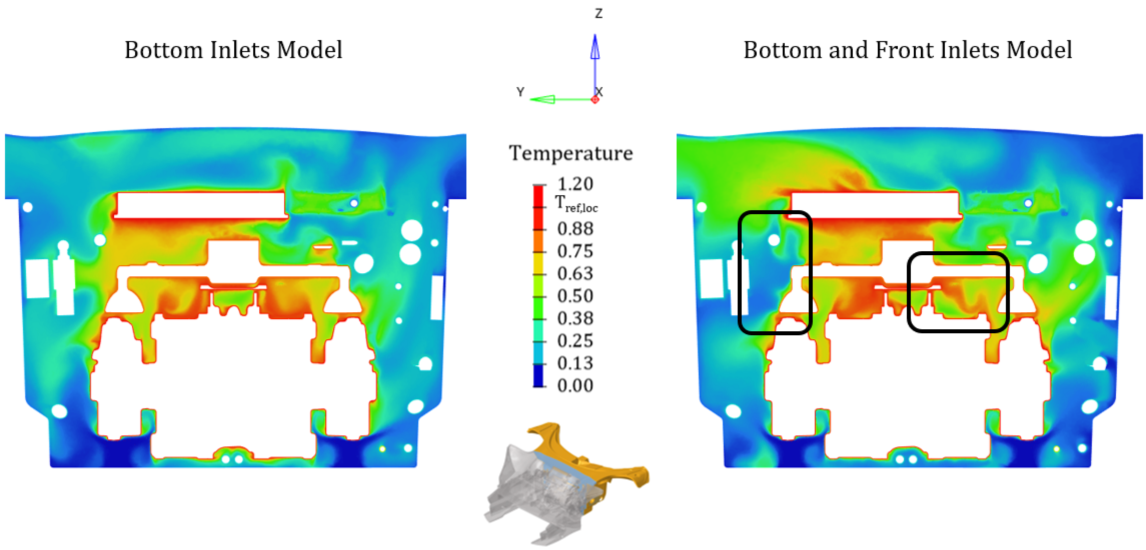

Figure 6.29: Local Target Temperature on Gearboxes, PDM unit and motors YZ section 1.

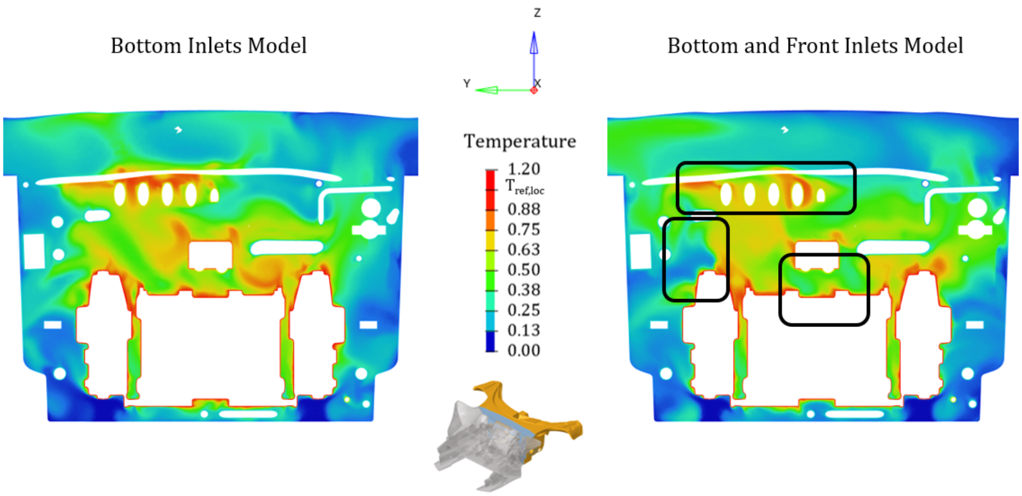

Figure 6.30: Local Target Temperature on Gearboxes, PDM unit and motors YZ section 2.

The other objective is to monitor the temperature around the TPMS sensor whose proper functioning is ensured when the ambient temperature does not exceed the limits specified by the constructor.

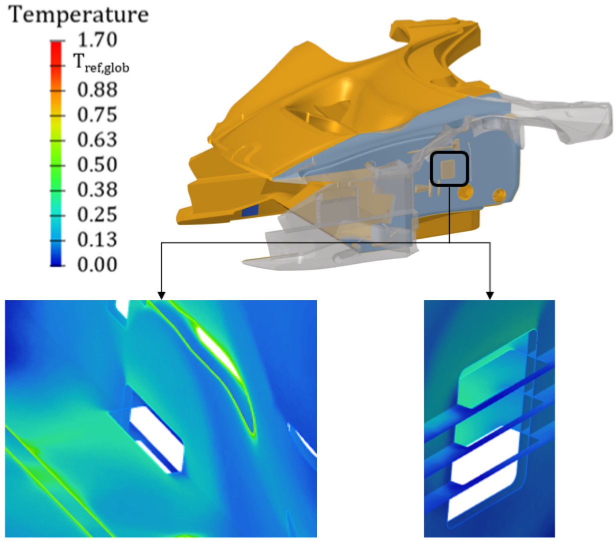

Figure 6.31: TPMS respect the Global Target Temperature.

As showed in the previous figure 6.31, the average temperature is less than 60% of $T_{max,TPMS}$ established by its company.

Moreover, it has been noted an interesting phenomenon about the outlet mass flows. As showed in the figure 6.32, both of them increase converging to an asymptotic value around $\dot{m} = 8\dot{m}_{ref}$ and the consequence is that stagnation pressure inlets -top and sides - reduce their own mass flow [Fig. 6.33].

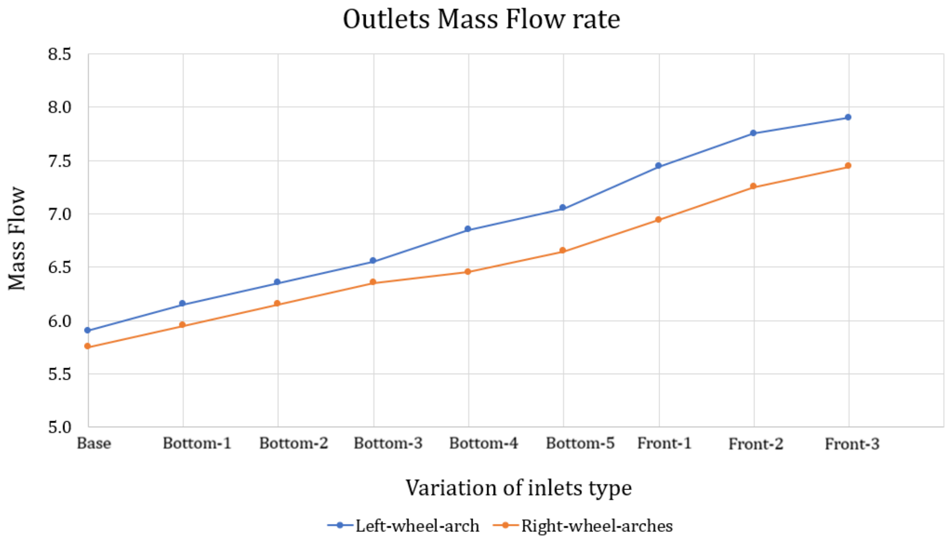

Figure 6.32: Outlets Mass Flow rates.

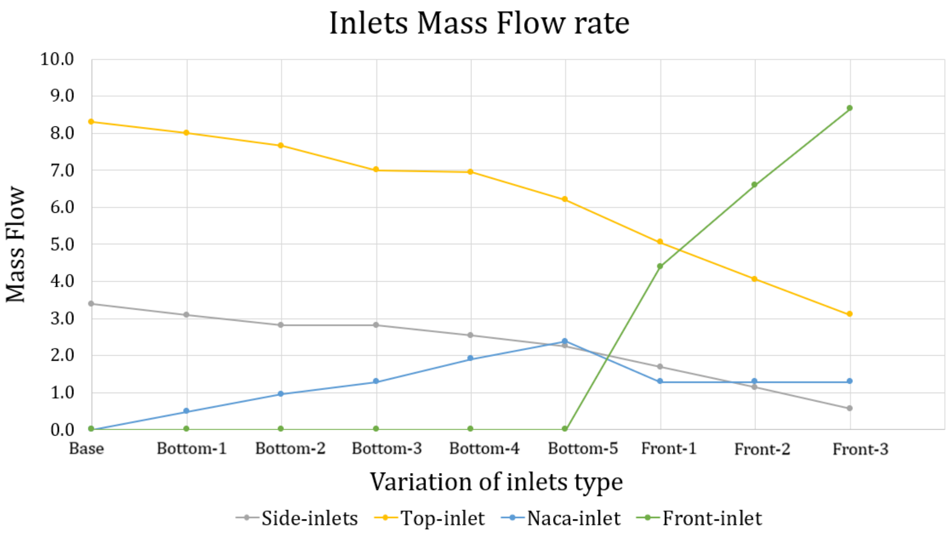

Figure 6.33: Inlets Mass Flow rates.

The outlets behave as they were spilling-over the airflow and the reason is the **System Resistance**. It is the resistance seen by air to move inside the compartment and it is not negligible due to the presence of so many close components.

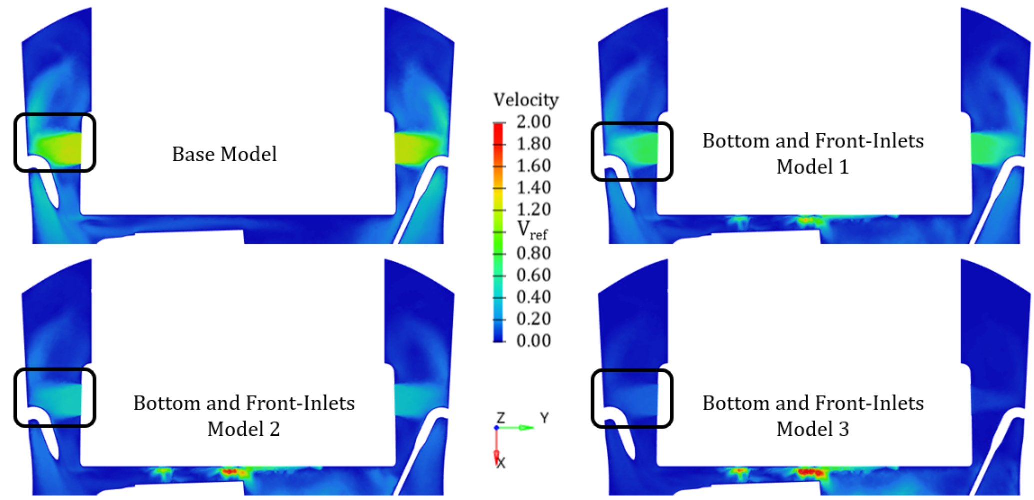

Figure 6.34: Side inlets velocity.

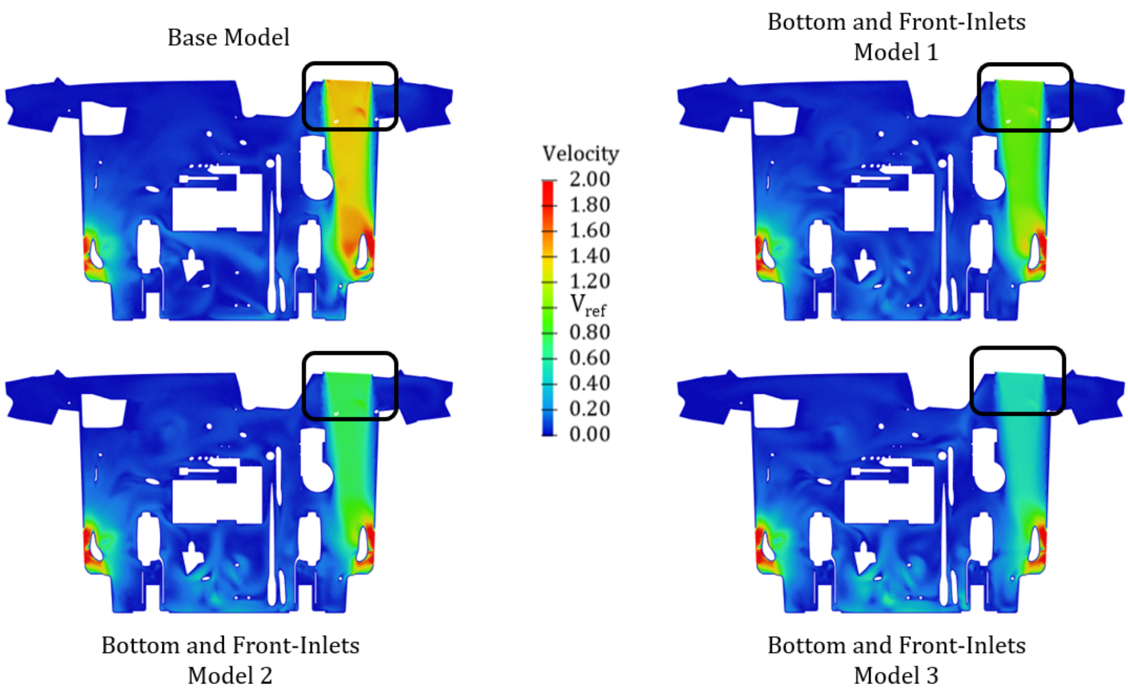

Figure 6.35: Top inlets velocity.

Chapter 7

Conclusions

In this thesis, the AcuSolve software, a CFD package that is part of the Altair Suite, was used to analyse and optimise the flowfield in the front powertrain compartment of the electric hypercar Rimac C_Two. This is important because, despite the temperatures in the underhood of an eletric hypercar being surely lower than those generated by an internal combustion engine, electric and electronic components have to work in a safe environment and they can be severely damaged by high temperatures. For this reasons the aim of this work was to evaluate the average temperature inside the powertrain compartment and ensure that the value was under the target, possibly implementing different solutions.

The pre-processing is based on the same logic of structural FEM analysis and this requires attention and time to generate a good quality mesh, especially in presence of many components. Indeed, the geometry has to be completely and properly closed, without showing any intersections among components and free edges that would prevent from generating the volume mesh. Moreover, AcuSolve demonstrated a strong sensitivity of the mesh which led easily to divergence and a specific remesher algorithm could help to prevent this situation. In addition, the software uses tetras as volume elements and this leads to increase easily the mesh and file size and of the file requiring a high level of computing resources. All these aspects are balanced for having this software already included in the Altair Suite without any added cost; therefore, studying in detail AcuSolve could be useful because it is already integrated in one of the main pre-processors on market.

Through this solver, the virtual simulations allowed to note as the air did not come out from the top opening but rather behaves as inlet, contrary to what was initially assumed. Thanks to these analysis it has been possible to indicate some feasible solutions (bottom and front additional inlets) in order to drive properly the design preventing possible serious thermal issues in the car. The virtual data showed an interesting phenomenon regarding the spill-over of airflow through the wheel-arches. This led to understand how the aforementioned improvements could not ensure enough airflow to cool the ambient temperature.

In order to achieve the goals completely, two options could be deepened:

- **Flow Splitters**, to force the airflow among the components reducing temperatures carrying out the generated heat ensuring always the correct operation;
- **Compartment Redesign**, to ensure the demand of target temperatures in any conditions it is possible to reposition some components, as moving in different place the hottest ones to decrease the system resistance seen by the airflow and allowing the cooling.

These solutions should be investigated further because, as demonstrated in cap. 6, they could reduce significantly the high system resistance developed by the components inside the compartment in this configuration.

The thesis highlighted the importance of testing a product by virtual analysis in order to prevent some critical issues. These could adversely affect the final performance and would be difficult to solve once produced. The use of software in this work represents an immense help to design properly leading to an almost ready product. In this way, it is possible to earn time in production phase and to avoid to waste capital in useless tests.

Acknowledgement

First of all, I would like to reserve a huge thank to my Academic Mentor, Prof. and Eng. Domenic D'Ambrosio, who has followed me during this educational experience helping me in critical situations that could be compromise this work and allowing to delivery it on time.

Following, I would like to thank immensely AMET and Rimac Automobili to allow me the chance to develop my thesis with them. Especially, I would like to show my profound acknowledgements to my AMET supervisors, Eng. Gabriele Velenich and Eng. Gianluca Francesconi in AMET, and CFD Manager of Rimac Automobili, Eng. David Sostaric. They have introduced me in the labour market conceding me the opportunity to ameliorate myself both personally and professionally. Despite facing new challenges, where the use of innovative tools was required, they consistently allowed this paper to be my own work, but steered me in the right direction whenever they thought I needed it providing the necessary support.

I would like to express my deepest gratitude to my parents who had always supporting me throughout my years of study spent between Lecce, Rome and Turin, especially in the last and stressful months. As I was ending this paper, Italy has been hit by COVID-19 pandemic and despite the distance they have given me continuously the strength to go ahead without giving up in the face of difficulties. They sacrificed themselves to allow me to study away from home and I will never be grateful enough for that.

In addition, a special thank is for my old friends and room-mates who supported me in the bad and good times that characterized last year,. Without their presence by my side, this incredible objective would have surely been more difficult to achieve.

Finally, I really would like to thank all my colleagues of Squadra Corse PoliTo - Turin Polytechnic Formula SAE Team. In the season 2018/19 we designed and produced a winning prototype and I am sure that also in the season 2019/20, without COVID-19 emergency, we would have been able to make the fastest car. I am thankful to everyone, from my Team Leader, Division Leader colleagues to my subordinates, because together we worked day and night trying to realize this project giving our best. Unfortunately, we will never see our dream driving on track but everyone has been fundamental for my growth, teaching how essential a good team work is to achieve something special. I will never forget you all.

Thanks to all of you.

Bibliography

[1] Amet, http://www.amet.it/activities, consulted on 20/02/2020.

[2] Altair, *AcuSolve 2019 Training Manual*, 2019.

[3] Anderson, J.D.Jr., *Computational Fluid Dynamics*, 1^{rd}, McGraw-Hill, Inc., USA.

[4] Ferziger, J.H., Peric, M., *Computational Methods for Fluid Dynamics*, 3^{rd}, Springer, Germany.

[5] Francesconi, G., *External Aerodynamics Optimisation using the Adjoint Method*, Master Thesis in Aerospace Engineering, Turin Polytechnic, 2018.

[6] Schlichting, H., Gersten, K., *Boundary-Layer Theory*, 9^{th}, Springer, Germany.

[7] Nanaki, E. A., Koroneos, C.J., *Climate change mitigation and deployment of electric vehicles in urban areas*, Renewable Energy, Elsevier, vol.99, December 2016.

[8] U.S. FDA, https://www.fda.gov/radiation-emitting-products/radiation-safety/electromagnetic-compatibility-emc, consulted on 14/03/2020.

[9] Deutschmann, B., Winkler, G., Kastner, P.,, E. A., Koroneos, C.J., *Impact of electromagnetic interference on the functional safety of smart power devices for automotive applications*, Elektrotechnik und Informationstechnik, July 2018.

[10] Cavagnino, A., Tenconi, A., Macchine elettriche - Aspetti termici, 2016.

[11] Rimac Automobili, https://www.rimac-automobili.com, consulted on 15/03/2020.

[12] Tosi, F., *Virtual Simulation for Clutch Thermal Behaviour Prediction*, Master Thesis in Aerospace Engineering, Turin Polytechnic, 2018.

[13] Brooks, A.N., Hughes, T.J.R., *Streamline upwind/Petrov-Galerkin formulations for convection dominated flows with particular emphasis on the incompressible Navier-Stokes equations*, North-Holland, 1982.

[14] Pope, S.B., *Turbulent Flows*, 1^{st} Cambridge University Press, 2000.

[15] P.R. Spalart, S. R.Allmaras, S. R., *A One-Equation Turbulence Model for Aerodynamic Flows*, AIAA Paper 92-0439, 1992.

[16] Lai, J,K., Merzari, E., Hassan, Y.A., *Sensitivity analyses in a buoyancy-driven closed system with high resolution CFD using Boussinesq approximation and variable density models*, International Journal of Heat and Fluid Flow, Elsevier, Vol. 75, 2019.

[17] Tritton, D.J., *Physical Fluid Dynamics*, 2^{nd}, Oxford Science Publications, 1988.

[18] Fiat Auto, Norma per la determinazione a calcolo della perdita di carico e dalla distribuzione della portata alle uscite di canalizzazioni aria., 2005.